iScience

CellPress
OPEN ACCESS

Article

The Mechanism of β2m Molecule-Induced Changes in the Peptide Presentation Profile in a Bony Fish

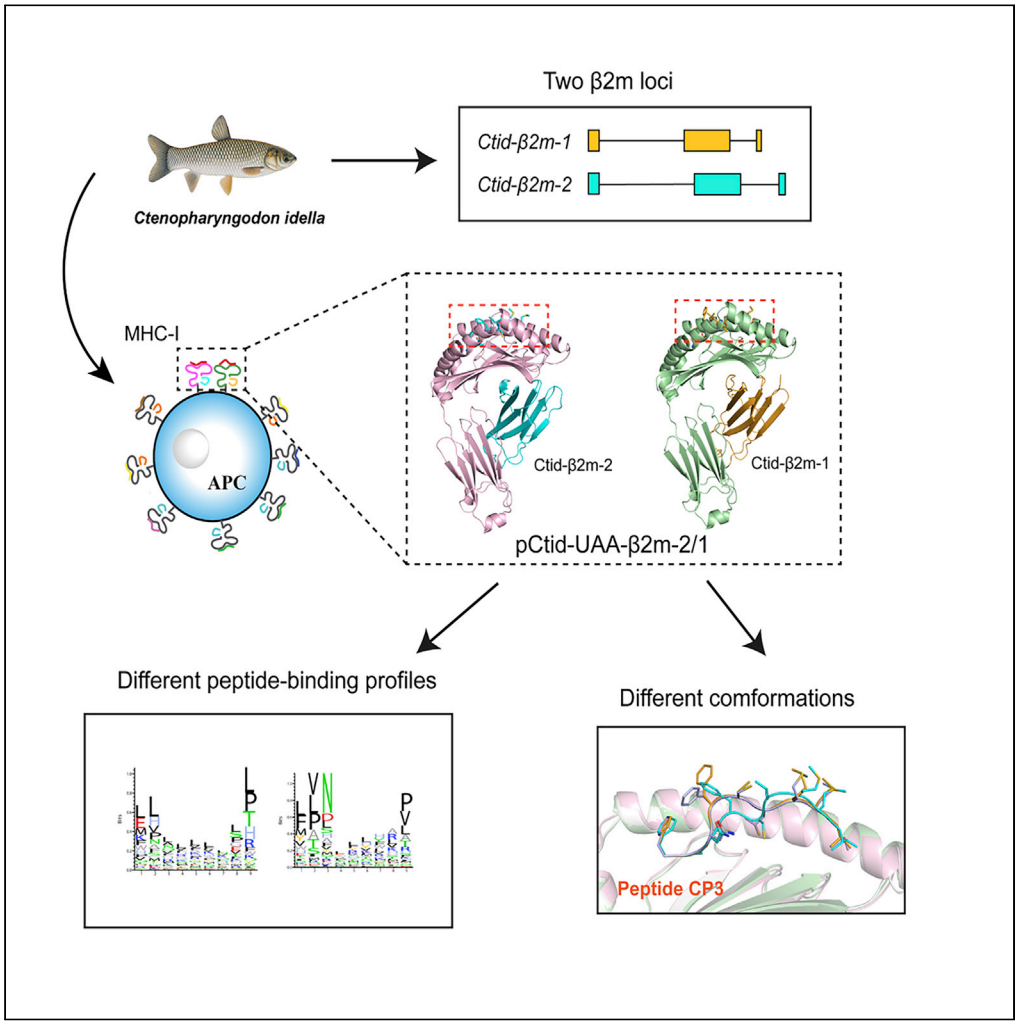

Zibin Li, Nianzhi Zhang, Lizhen Ma, Lijie Zhang, Geng Meng, Chun Xia

xiachun@cau.edu.cn

HIGHLIGHTS

Two Ctid-β2ms loci with distinct polymorphic features are found in a bony fish

The pMHC-I complexes peptide-binding profiles exhibit different characteristics

The crystal structures of pCtid-UAA-β2m-2/1-II complexes are determined

The structural mechanism changing the peptide presentation profile is proposed

DATA AND CODE AVAILABILITY

6LBE
5H5Z

Li et al., iScience *23*, 101119
May 22, 2020
https://doi.org/10.1016/j.isci.2020.101119

iScience

CellPress
OPEN ACCESS

Article

The Mechanism of β2m Molecule-Induced Changes in the Peptide Presentation Profile in a Bony Fish

Zibin Li,[1,3] Nianzhi Zhang,[1,3] Lizhen Ma,[1] Lijie Zhang,[1] Geng Meng,[2] and Chun Xia[1,4,*]

SUMMARY

Contemporary antigen presentation knowledge is based on the existence of a single β2m locus, and a classical MHC class I forms a complex with a peptide (i.e., pMHC-I) to trigger CTL immunity. However, two β2m loci have been found in diploid bony fish; the function of the two β2m molecules is unclear. Here, we determined the variant peptide profiles originating from different products of the β2m loci binding to the same MHC-I molecule and further solved the crystal structures of the two pMHC-I molecules (i.e., pCtid-UAA-β2m-2 and pCtid-UAA-β2m-1-II). Of note, in pCtid-UAA-β2m-2, a unique hydrogen bond network formed in the bottom of the peptide-binding groove (PBG) led to α2-helix drift, ultimately leading to structural changes in the PBG. The mechanism of the change in peptide presentation profiles by β2m molecules is illustrated. The results are also of great significance for antivirus and antitumor functions in cold-blooded vertebrates and even humans.

INTRODUCTION

β2-Microglobulin (β2m), which contains only one basic immunoglobulin superfamily C1-set fold (i.e., IgSF-C1), has been found in the adaptive immune system (AIS) of jawed vertebrates (Cooper and Alder, 2006). The immunological function of β2m is to assist classical major histocompatibility complex (MHC) class I (i.e., MHC-I) molecules in assembling endogenous antigen peptides, forming a trimolecular complex (i.e., pMHC-I) and then presenting them to the surface of antigen-presenting cells (APCs); through interaction with T cell receptors (TCRs), specific cytotoxic T lymphocyte (CTL) immunity is thus induced (Flajnik and Kasahara, 2001). In addition to classical MHC-I molecules, β2m can also associate with nonclassical MHC-I molecules, such as the CD1 molecule and the α chain of the Fc receptor for IgG, playing important biological roles in the AIS (Simister and Mostov, 1989). Existing knowledge indicates that some cold-blooded vertebrates, such as fishes, amphibians, and reptiles, and warm-blooded vertebrates, such as birds and mammals, have only one β2m locus in their genomes (International Chicken Genome Sequencing Consortium, 2004; Lappalainen et al., 2019), although there are exceptions (Ohta et al., 2011). In addition, the β2m alleles expressed by the one locus have no polymorphism and play equal immunological roles, as mentioned above. Thus far, in the immune system of jawed vertebrates, the invariable β2m and polymorphic MHC-I molecules form a very clear coevolutionary relationship; when a lack or knockout of the β2m gene occurs, the CTL immune response becomes invalid (Kumar and Hedges, 1998). In addition, a large amount of β2m molecule release from pMHC-I complexes will also lead to a variety of serious diseases (Zhang et al., 2019).

It is generally believed that the β2m association with MHC-I molecules initially arose in primary jawed vertebrates and is encoded by a single locus outside of the MHC region in almost all species (Goodfellow et al., 1975; Robinson et al., 1981). In only one exception, β2m was found to be linked to the primordial MHC region in a cartilaginous fish (Ohta et al., 2011). In most higher vertebrates, individuals possess multiple MHC-I loci with high polymorphism, but only one invariant β2m gene is encoded by a single locus, which is distant from the MHC region (Hurlbut, 2019; Rubin et al., 2010; Session et al., 2016). Only a limited allelic polymorphism of the single β2m locus has been found among different mouse individuals (Gates et al., 1981; Robinson et al., 1981). However, in cold-blooded vertebrates, such as fish, their MHC-I genes are more complicated, with high levels of recombination and gene conversion, and the accumulation of whole-genome sequences has led to delineation of multiple MHC-I lineages (Flajnik, 2018; Grimholt, 2016, 2018).The majority of studies about fish β2ms mainly focused on the molecular level; however, limited functional explorations were reported based on viral infection model in fish (Chen et al., 2010b; Sever et al., 2014). A general knowledge is that the number of β2m loci varies a lot between fish species. For example, rainbow trout has at least three, one of which is presumed to be a

[1]Department of Microbiology and Immunology, College of Veterinary Medicine, China Agricultural University, Beijing, 100193, China

[2]Beijing Advanced Innovation Center for Food Nutrition and Human Health, College of Veterinary Medicine, China Agricultural University, Beijing, 100094, China

[3]These authors contributed equally

[4]Lead Contact

*Correspondence: xiachun@cau.edu.cn

https://doi.org/10.1016/j.isci.2020.101119

pseudogene, but there are many others in the trout genome (Magor et al., 2004; Shum et al., 1996). There is only one copy in the walleye genome (Christie et al., 2007) and one copy in tilapia but two in carp (Dixon et al., 1993; Ono et al., 1993). Interestingly, two striking features were found in bony fish β2m genes, compared with those of other species: first, they exhibit multiple copy numbers and polymorphisms, which are correlated with ploidy levels (Dixon et al., 1993; Hao et al., 2006; Lundqvist et al., 1999). Notably, the β2m genes of rainbow trout are a special case that does not conform to the mammalian paradigm; ten of twelve randomly selected β2m cDNA clones from an individual fish were found to show different nucleotide sequences, and fragment length polymorphism patterns suggested that multiple β2m genes exist in the genome (Shum et al., 1996). In addition to the known β2m, a second type of β2m molecule has been found in marine fish (Kondo et al., 2010). Genome-wide scans of high-quality genome assemblies from deep sequencing have confirmed the presence of some genes annotated as β2m in Cyprinidae fishes, such as the grass carp (*Ctenopharyngodon idella*), suggesting the existence of a second β2m locus, i.e., two loci exist in its genome (Howe et al., 2013; Xu et al., 2014). Furthermore, the sequence similarity between the two loci is low (Kondo et al., 2010). However, it is unclear how this diverse and polymorphic β2m collaborates with MHC-I molecules to present peptide antigens.

A turning point is that we first clarified the grass carp pMHC-I structure (i.e., pCtid-UAA) (Chen et al., 2017). The structural mechanism of presenting antigen peptides via bony fish β2m and MHC-I complexes has been analyzed. The function of β2m includes noncovalent binding to MHC-I, which stabilizes the three-dimensional (3D) structure of the pMHC-I complex (Lancet et al., 1979), assisting in T cell activation and CTL immunity (Jondal et al., 1996). On this basis, we are interested in the function of the two β2m loci, especially the second β2m locus, which is a very rare phenomenon in immunology that may exhibit novel characteristics. How do the products of the two β2m loci, whose amino acid sequence difference is so direct, present antigen peptides? This special scientific question in cold-blooded vertebrates has great value.

In this study, the grass carp Ctid-β2m genes from the two loci were cloned, classified, and expressed. The already known locus Ctid-β2m (i.e., Ctid-β2m-1) is polymorphic and can be divided into two subgroups, Ctid-β2m-1-I and Ctid-β2m-1-II. The second type of Ctid-β2m (i.e., Ctid-β2m-2) was also identified in the carp genome and cDNA. The expression levels of the two types of Ctid-β2ms were highly similar across most tissues from normal individuals. Moreover, Ctid-β2m-2, Ctid-UAA, and an epitope peptide were assembled into a pMHC-I complex similar to that of Ctid-β2m-1 (Chen et al., 2017). The peptide-binding profiles of the three pMHC-I complexes were determined by mass spectrometry. The crystal structures of pCtid-UAA-β2m-2 and pCtid-UAA-β2m-1-II binding to the same peptide were solved. Upon comparing the two types of pCtid-UAA-β2m structures, we found that Ctid-β2m-1 and Ctid-β2m-2 interacted with MHC-I/Ctid-UAA in different ways, resulting in two kinds of peptide-binding grooves (PBGs) while also presenting the same peptide in different conformations. According to these results, both the Ctid-β2m-1 and Ctid-β2m-2 genes are able to participate in the assembly of pMHC-I complexes, and the mechanism of the change in peptide presentation profiles by β2m molecules was illustrated. The results also implied that artificial alteration of the β2m sequence can change its peptide-binding profile, which is of great significance in the study of antivirus, antitumor functions in mammals.

RESULTS

Two Branches of β2ms from Two Loci Are Broadly Expressed in Various Tissues

The alleles of Ctid-β2m-2 and the previously identified Ctid-β2m-1 (-I and -II) genes (Chen et al., 2010a; Wang et al., 2015) were located in two separate regions on the carp genome (scaffold CI01000020). The gene organization of Ctid-β2m-1 and Ctid-β2m-2 comprised three coding exons and two introns within a 1.048- and 1.33-kb genomic fragment, respectively (Figure 1A); both genomic structures of exons and introns were fundamentally similar. A pair of specific primers was designed to amplify the Ctid-β2m-2 gene from the carp cDNA (Hao et al., 2006). A 354-bp gene fragment was obtained. To determine whether the two types of Ctid-β2m genes had tissue-specific expression, RNAs from different grass carp tissues were collected and the expression levels were measured with a real-time RT-PCR assay. The expression levels of the two types of Ctid-β2m genes showed no significant differences among tissues (Figure 1B), and both types were broadly expressed in grass carp tissues.

To assess the polymorphism of the two Ctid-β2m loci, primers were designed based on the two Ctid-β2m gene sequences to amplify different alleles from cDNAs. Their individual and corresponding gene sequence information are listed in Table S1. In contrast, the cloned Ctid-β2m-2 sequences from 11 outbred grass carps were identical, which indicated that the Ctid-β2m-2 gene is highly conserved in different individuals. In contrast, each diploid grass carp individual had two different Ctid-β2m-1 alleles, and 9 new alleles were cloned from 11 individuals, suggesting that Ctid-β2m-1 genes are highly polymorphic in different individuals. Phylogenetic analysis

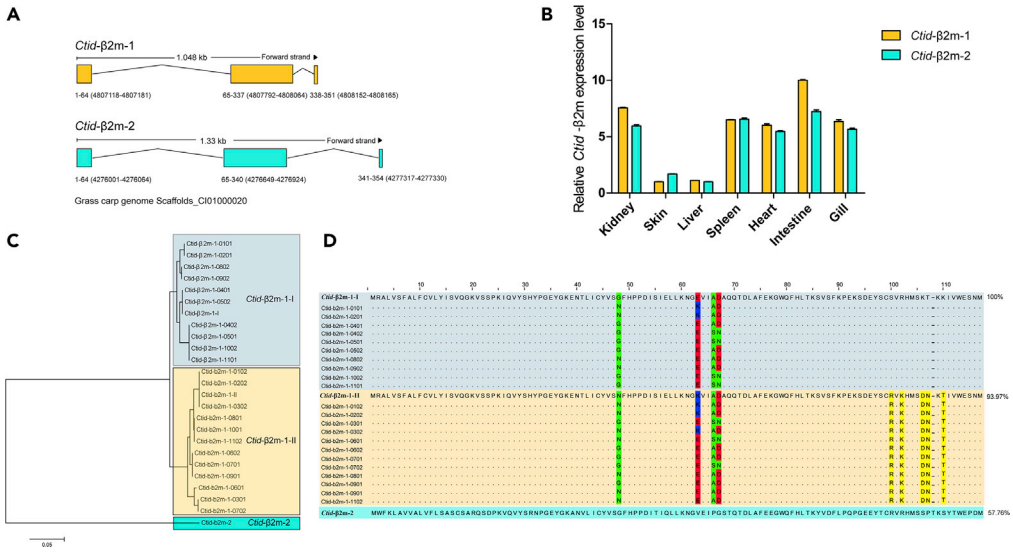

Figure 1. Systematic Analysis of Grass Carp β2ms

(A) Genomic structures of grass carp β2m genes (Ctid-β2m-2 and Ctid-β2m-1). The two types of Ctid-β2ms are located on the grass carp genome scaffold CI01000020. The loci consist of three coding exons of the same size and two introns of different sizes.

(B) mRNA expression levels of the two types of Ctid-β2ms in different tissues (kidney, skin, liver, spleen, heart, intestine, and gill) of the grass carp. The values are expressed as the means ± SEMs.

(C) A phylogenetic tree based on the amino acid sequences of the alleles of the two types of Ctid-β2ms from 11 fish was constructed using the neighbor-joining method.

(D) Two Ctid-β2m-1-I/II alleles and a conserved Ctid-β2m-2 can be cloned from diploid grass carp. Nine new Ctid-β2m-1 alleles were identified from 11 grass carp individuals (Table S1). Alignment of amino acid sequences of the two types of Ctid-β2ms from 11 grass carp individuals. The sequence similarity between Ctid-β2m-1-I and Ctid-β2m-1-II is approximately 94%, and the sequence similarity between Ctid-β2m-1-I and Ctid-β2m-2 is approximately 58%. The discrepant acidic amino acids and basic amino acids are indicated with red and blue, respectively, and the others are shaded in green. Specific notable sequences (i.e., RKDNT) are shaded in yellow in Ctid-β2m-1-II.

of the two Ctid-β2m genes showed that the obtained Ctid-β2m-1 and Ctid-β2m-2 sequences clustered into two branches (Figure 1C) and that the Ctid-β2m-1 alleles were further divided into two subgroups (-I and -II), consistent with our previous report (Hao et al., 2006). An alignment of the full-length amino acid sequences of the two Ctid-β2ms from 11 individuals is shown (Figure 1D). The Ctid-β2m-1-I/II showed high sequence similarity of greater than 92%; the variable amino acid sites were located at positions 48, 63, 66, and 67. Notably, a cluster of conserved amino acid sites (i.e., RKDNT) was found in Ctid-β2m-1-II. In contrast, Ctid-β2m-2 had only low sequence similarity with Ctid-β2m-1 (approximately 57.8%).

The Two Kinds of β2ms Participate in pMHC-I Complexes and Show Different Peptide-Binding Profiles

A random nonapeptide library *in vitro* binding assay was performed to confirm the antigen-presenting functions for each Ctid-β2m. With random nonapeptides, both Ctid-β2ms could assemble into a pMHC-I structure (Figures 2A and 2B). Subsequently, the bound random nonapeptides were analyzed for the two types of pCtid-UAA-β2m complexes (Table S2). The peptide-binding profiles for the pCtid-UAA-β2m-1-I and pCtid-UAA-β2m-1-II complexes were mostly consistent, and the motif from the peptide (i.e., CP3) matched well with both profiles (Figure 2C). Furthermore, our previous report showed that the D pocket of pCtid-UAA-β2m-1-I was critical for antigen binding, where P3-N was fixed as the primary anchor residue (Chen et al., 2017). In these results, P3-N appeared as the predominant anchor residue on the two pCtid-UAA-β2m-1 complexes (Figure 2C). Therefore, to a certain extent, this assay was relatively reliable and could reflect this feature of the pCtid-UAA-binding peptides. However, compared with that of pCtid-UAA-β2m-1, the peptide-binding profile of pCtid-UAA-β2m-2 displayed different characteristics: P3-N lost its status as the predominant anchor residue. In addition to changes in P3 residues, the residue preferences of other positions significantly changed (Figure 2C). The binding peptides were very different

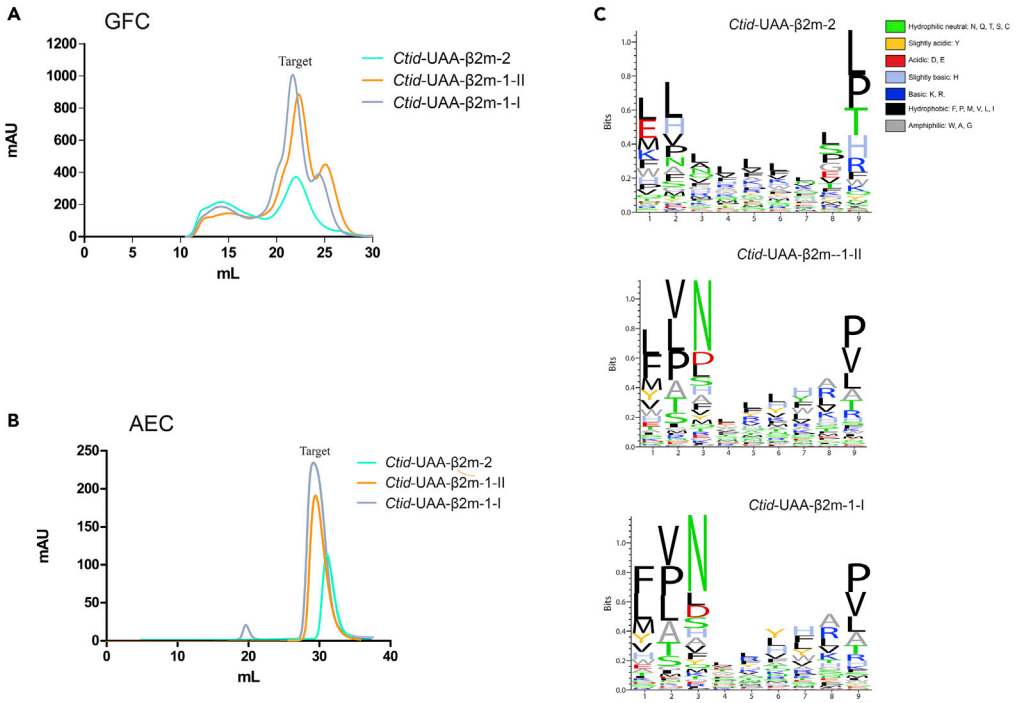

Figure 2. Random Nonapeptide Library *In Vitro* Binding Assays

(A and B) Gel filtration chromatography (GFC) and anion exchange chromatography (AEC) profiles of the refolded products of the two types of Ctid-UAA-β2ms.

(C) Sequence logo plots of the binding of amino acid motifs by the two types of Ctid-UAA-β2ms to a random nonapeptide library. Nonapeptide ligands identified with an LC-MS/MS de novo method for the two types of Ctid-UAA-β2ms were analyzed by Seq2Logo 2.1. The Shannon presentation type was used, and the other parameters were set as the default values. The numbers below the axis represent the different nonapeptide positions. The amino acids are shown in different colors according to their chemical properties.

from those of the two pCtid-UAA-β2m-1 complexes. These results indicated that the different Ctid-β2ms, i.e., β2m-1 and β2m-2, undoubtedly influenced the peptide-binding profile.

Crystal Structures of the Two Kinds of pMHC-I Complexes

Ctid-UAA, Ctid-β2m-2, and the peptide CP3 were assembled. After refolding and purification, a trimer complex (i.e., pCtid-UAA-β2m-2) was obtained (Figures S1A and S1B), and the pCtid-UAA-β2m-1-II complex was obtained for Ctid-β2m-1-II (Figures S1C and S1D). To determine the differences between the two kinds of pCtid-UAA-β2m complexes, the structures of the pCtid-UAA-β2m-2 and pCtid-UAA-β2m-1-II complexes bound to the same peptide were determined. The data collection and refinement statistics are shown in Table 1. Both the pCtid-UAA-β2m-2 and pCtid-UAA-β2m-1-II complexes displayed a canonical pMHC-I structure, in which the peptide CP3 was located in the PBGs formed by the α1 and α2 domains and the α3 domains controlled primarily the binding of the two distinct Ctid-β2ms (Figure 3A). The pCtid-UAA-β2m-2/1-II complexes were then superimposed on the reported pCtid-UAA-β2m-1-I complex (Chen et al., 2017), and it was clear that the pCtid-UAA-β2m-2 complex had more significant overall structural differences than the pCtid-UAA-β2m-1-II and pCtid-UAA-β2m-1-I complexes; the corresponding root-mean-square deviation (RMSD) values were 0.868 and 0.153, respectively (Figure 3A).

Two types of Ctid-β2m-2 and Ctid-β2m-1-II monomer structures were clearly displayed (Figure 3B). Similar to the known Ctid-β2m-1-I monomer, Ctid-β2m-2 and Ctid-β2m-1-II were composed of 99 and 98 mature residues, respectively; had a seven-stranded β-sandwich fold; and belonged to the typical IgSF-C1 group of molecules. A conserved central disulfide bond bridging the C25 and C80 positions of the B and F strands contributed to overall monomer structural stability. Although Ctid-β2m-2 shared low amino acid similarity with Ctid-β2m-1-I and Ctid-β2m-1-II, it could maintain a topology similar to that of Ctid-β2m-1-I after binding Ctid-UAA. However,

	Ctid-UAA-β2m-2 (6LBE)	*Ctid*-UAA-β2m-1-II (5H5Z)
Data Collection		
Space group	P1	C121
Cell dimensions		
a, *b*, *c* (Å)	53.19, 65.27, 69.71	119.3, 50.6, 90.3
α, *β*, *γ* (°)	64.94, 75.67, 73.61	90, 90, 90
Resolution (Å)	62.46–2.60	50.00–1.74
*R*merge (%)	20.5 (68.4)	8.2 (42.3)
$I/\sigma I$	17.86 (2.33)	17.5 (3.2)
Completeness (%)	82.1 (81.8)	98.4 (98.3)
Redundancy	2.3(1.9)	4.5 (4.7)
Refinement		
Resolution (Å)	62.46–2.60	50.00–2.10
No. reflections	20,364	27,016
R_{work}/R_{free}	0.169/0.254	0.176/0.204
RMS deviations		
Bond lengths (Å)	0.012	0.010
Bond angles (°)	1.37	1.030
Average B factor	27.69	32.85
Ramachandran plot quality		
Most favored region (%)	96.89	97.87
Allowed region (%)	3.11	2.13
Disallowed (%)	0.0	0.0

Table 1. Data Collection and Refinement Statistics (Molecular Replacement)
Values in parentheses are for highest-resolution shell.

some subtle differences could still be found, as supported by the RMSD value (0.469) (Figure 3B). Unlike those of Ctid-β2m-1, the variable amino acids of Ctid-β2m-2 were distributed throughout the structure and were mainly concentrated in the conformational difference regions, i.e., the CD loop, EF loop, and G strand (Figure S2). In contrast, Ctid-β2m-1-II, as a member of the Ctid-β2m-1 subgroup, shared high sequence similarity with Ctid-β2m-1-I (Figure 3C) and could essentially maintain a conformation consistent with that of Ctid-β2m-1-I; the RMSD value was 0.157 (Figure 3B). However, as before, we found a cluster of conserved amino acids (i.e., RKDNT) distributed on the F and G strands that did not contact Ctid-UAA.

Ctid-β2m-1 and Ctid-β2m-2 Utilize Different Ways to Form pMHC-I Complexes

The main interactions between the two types of Ctid-β2ms and Ctid-UAA were compared and are listed in Tables S3 and S4. A total of 24 hydrogen bonds and 12 salt bridges between Ctid-β2m-2 and Ctid-UAA, which is greater than that for the pCtid-UAA-β2m-1-I and UAA-β2m-1-II complexes, were found. The interactions between the two types of Ctid-β2ms and the Ctid-UAA were focused mainly in four areas (Figures 4A and 4B). As expected, in the pCtid-UAA-β2m-1-II complex, the composition and conformation of the residues involved in the interactions were essentially identical to those in the pCtid-UAA-β2m-1-I complex, except that D34 replaced I35 (see BC loop, Ctid-β2m-1-I) and formed a hydrogen bond with D17 (see AB loop, Ctid-UAA) and two additional hydrogen bonds were formed between S95/M97 (tail loop, Ctid-β2m-1-II) and K188 (α3 tail, Ctid-UAA). In contrast, in the pCtid-UAA-β2m-2 complex, Ctid-β2m-2 and Ctid-UAA adopted a distinct interaction mode in which multiple variable amino acids were involved in the

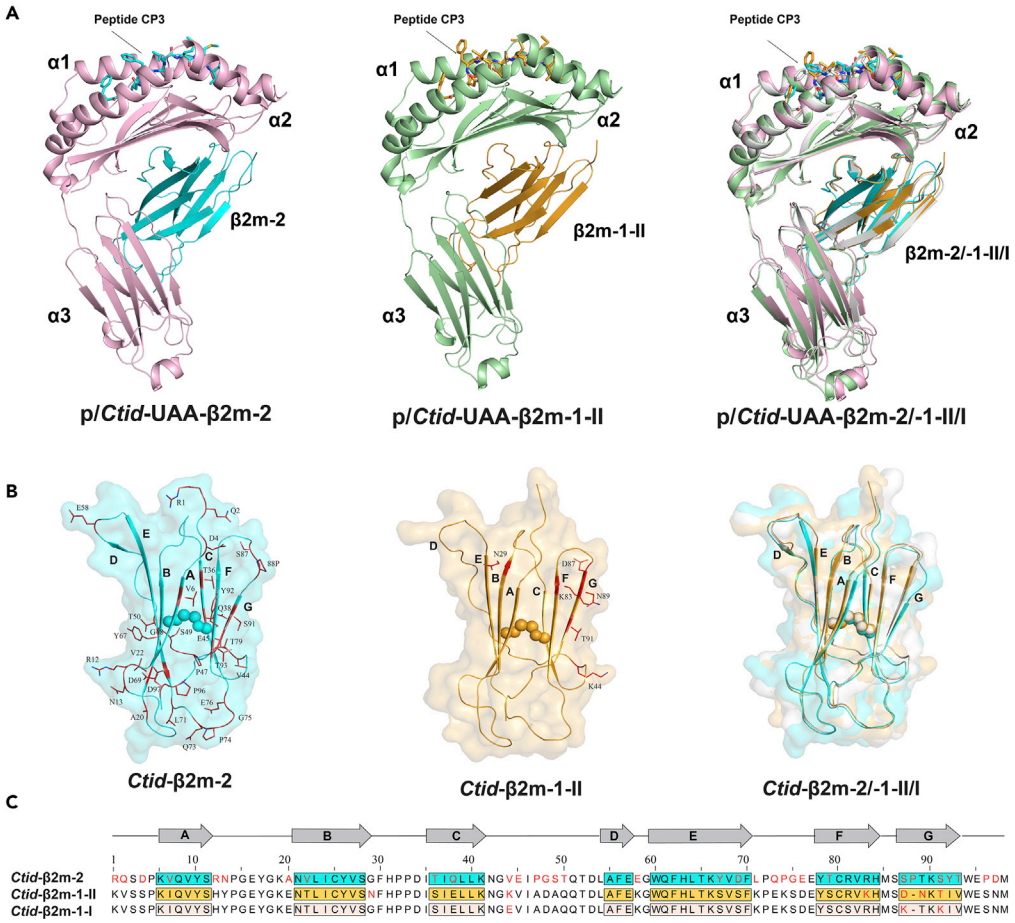

Figure 3. Overall Structures and Comparison of the Two Types of pCtid-UAA-β2ms

(A) The overall structures of the pCtid-UAA-β2m-2 and pCtid-UAA-β2m-1-II complexes are shown as cartoons colored cyan and orange, respectively. Both complexes are superimposed onto pCtid-UAA-β2m-1-I, and the overall structure of pCtid-UAA-β2m-1-I is colored white.

(B) The monomer structures of Ctid-β2m-2 and Ctid-β2m-1-II are colored cyan and orange, respectively. They show a typical IgSF-C1-type architecture. The β strands are labeled with the letters A to G. The conserved disulfide bonds formed between C24 and C79 are shown as spheres, and the variable amino acid sites of Ctid-β2m-2 and Ctid-β2m-1-II are shown as sticks and labeled. Both Ctid-β2m-2 and Ctid-β2m-1-II are superimposed onto Ctid-β2m-1-I, and the monomer structure of Ctid-β2m-1-I is colored white.

(C) Alignment of the amino acid sequences of the two types of Ctid-β2ms. The discrepant amino acids in the two types of Ctid-β2ms are indicated in red. Their different β-strand segments are boxed in the corresponding colors.

interactions and played a crucial role. In the **a** area, an additional hydrogen bond was formed by D58 (DE loop, Ctid-β2m-2) and Q111 (PBG, Ctid-UAA) in pCtid-β2m-2, which is absent in pCtid-β2m-1-I/II. In the **b** area, no variable amino acids participated in the interaction. However, two additional hydrogen bond networks were formed between H31 in the BC loop of Ctid-β2m-2 and T91 at the bottom of the PBG of pCtid-UAA and between D34 in the BC loop of Ctid-β2m-2 and I16 in the AB loop of Ctid-UAA; furthermore, an additional salt bridge was formed between R83 in the F strand of Ctid-β2m-2 and D17 in the AB loop of Ctid-UAA. In the **c** area, the variable amino acid E58 in the DE loop of Ctid-β2m-2 and Q111 at the bottom of the PBG of pCtid-UAA formed a hydrogen bond, whereas the other interactions were identical to those found in the pCtid-UAA-β2m-1-I complex. In the core **c** area, the variable amino acid R12 in the AB loop of Ctid-β2m-2 initiated an intricate hydrogen bond and salt bridge network (in α3 of pCtid-UAA) that involved seven amino acids, namely, Q183, H197, T199, E230, D231, S233, and Q235. The remaining interactions were consistent with those found in the two pCtid-UAA-β2m-1 complexes. In the **d** area, an additional salt bridge was formed between the variable amino acid D97 (in the tail loop of Ctid-β2m-2) and K188

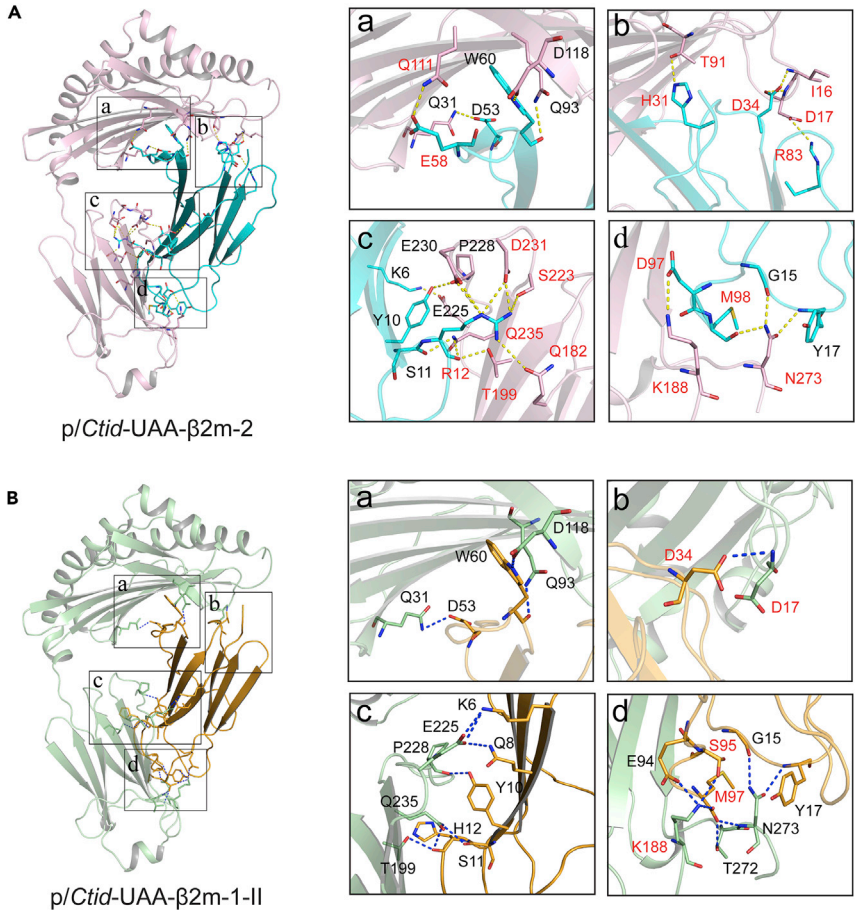

Figure 4. Comparison of the Interactions between the Heavy Chain and the Light Chains in the Two Types of pCtid-UAA-β2ms

(A and B) Interactions between the heavy chain (HC) and the light chains (LCs) in pCtid-UAA-β2m-2 and pCtid-UAA-β2m-1-II. In pCtid-UAA-β2m-2, the Ctid-UAA HC is colored pink and the Ctid-β2m-2 LC is colored cyan. In pCtid-UAA-β2m-1-II, the Ctid-UAA HC is colored light green and the Ctid-β2m-2 LC is colored orange. Interactions occur mainly in four areas (a–d). In these areas, the hydrogen bonds and salt bridges in pCtid-UAA-β2m-2 and pCtid-UAA-β2m-1-II are shown as yellow and blue dashed lines, respectively. The labeled interacting residues are shown as sticks and are colored according to the atom types (blue, N; red, O). The specific interacting residue positions that differ from those of pCtid-UAA-β2m-1-I are labeled red in the four areas of pCtid-UAA-β2m-2 and pCtid-UAA-β2m-1-II.

(in the α3 tail of pCtid-UAA). Furthermore, M98 (in the tail loop of Ctid-β2m-2) also formed an additional hydrogen bond with N273 (in α3 of pCtid-UAA).

In addition, our previous study showed that the area of the interface between the Ctid-β2m-1-I and the Ctid-UAA was 1744 Å2, which was the largest interface area of all solved pMHC-I structures (Chen et al., 2017). We analyzed the interface areas for the pCtid-UAA-β2m-2 and pCtid-UAA-β2m-1-II complexes and found them to be 1728 and 1746 $Å^2$, respectively (Figure S3), which are almost identical to that for the pCtid-UAA-β2m-1-I complex.

The Structural Mechanism of Ctid-β2m Changing the Peptide Presentation Profile

Despite some of the above-described differences, the key region involved in the interaction between Ctid-β2m and the PBG in pCtid-UAA is shown in Figure 4. The conserved W60 residue in the DE loop of Ctid-β2ms participated in forming two hydrogen bonds with Q93 and D118 and played a crucial role in maintaining the overall conformational stability of the PBG. However, in the pCtid-UAA-β2m-2 complex, a unique hydrogen bond formed between E58 in the DE loop of Ctid-β2m-2 and Q111 at the bottom of the PBG that skewed the DE loop and led to a corresponding change in the relative position of W60 (Figure 5A). Furthermore, the shift of W60 led to the α2.1 helix

and the surrounding region shifting to the outside (Figure 5A), which in turn led to structural changes in the entire PBG of pCtid-UAA-β2m-2; accordingly, the changed pockets could accommodate different peptides (Figure 2C). Upon comparing the conformation of the six pockets of pCtid-UAA-β2m-2 accommodating the peptide, we found that a shift (~1.2 Å) in the α2.1 helix led to changes in the relative positions of T139, K142, and W143, which constitute the F pocket. In addition, the C pocket of pCtid-UAA-β2m-2 became deeper than those of the two pCtid-UAA-β2m-1 complexes. In the pCtid-UAA-β2m-1 complexes, the side chain of F72 was positioned toward the inner side of the PBG, whereas it was skewed 114.2° toward the outside of the PBG in pCtid-UAA-β2m-2 (Figure 5B).

The differences in the interactions between the peptide and the PBGs that led to conformational changes are shown in Figure 5C. Notably, the peptide conformations of the two pCtid-UAA-β2m-1 complexes (-I and -II) were essentially the same. However, the peptide conformation of pCtid-UAA-β2m-2 was significantly different from that of the other two complexes. First, the whole peptide conformation shifted by approximately 2.6 Å at the P4-F position. Second, the orientation of P5-C and P6-L was reversed; the main chain of the peptide turned sharply into the bottom of the PBG at the P5-C position and then rose at P6-L. Moreover, the B factor values of peptide in the two types of pCtid-UAA-β2m complexes were analyzed, and the peptide was elongated in the PBG (Figure 5D). Therefore, these facts undoubtedly signify changes in their peptide-binding profiles (Figure 2C). The structural changes in the PBG were consistent with an impact on the interactions between the peptide CP3 and the PBG. In the two types of pCtid-UAA-β2m complexes, the interactions between the peptide CP3 and the PBG were analyzed (Figure S4). In the pCtid-UAA-β2m-2 complex, the loss of a main-chain hydrogen bond formed between P9-I and K142 occurred, which was replaced with an additional side chain hydrogen bond formed between P9-I and R82 (Figure 5E). In addition, the side chains of P3-I and Q151 also formed a hydrogen bond. In contrast, in pCtid-UAA-β2m-1-II, the hydrogen bonds between the peptide and the PBG were identical to those found in pCtid-UAA-β2m-1-I (Figure 5F).

Ctid-β2m-2 Has Conserved Amino Acid Motifs Involved in the Interaction with Ctid-UAA

The β2m is a crucial subunit of the pMHC-I complex, and its main function is to participate in the pMHC-I interaction and maintain structural stability. Therefore, we presumed that amino acids involved in the interaction with MHC-I should be retained during evolution and may be present in the two types of Ctid-β2ms. Based on the resolved representative pMHC-I complexes of different species, the amino acids of β2m that can interact with MHC-I are shown (Figure 6). Eight conserved amino acid motifs (Q8, Y10, S11, R12, H31, D53, W60, and D97/98) were identified, which are widely present in mammals and birds. In birds, D98 is replaced by an E, but the charge of the two residues is identical. However, Ctid-β2m-2 retained this conserved amino acid motifs, compared with Ctid-β2m-1 (Figure 6A). In Ctid-β2m-1, R12 is mutated to an H and D96 is mutated to an N, whereas H31 does not participate in the interaction with Ctid-UAA.

DISCUSSION

Existing knowledge of classical MHC-I antigen presentation is based on the existence of a single copy of β2m, that is, MHC-I forms a complex with a single β2m and a peptide to restrictively trigger CTL immunity (Jondal et al., 1996). In addition, the different peptide profiles are mainly due to the polymorphism of alleles in different MHC-I loci, which is unrelated to β2m because β2m, also known as the MHC-I light chain, has no polymorphism and functions only to stabilize pMHC-I (Bjorkman et al., 1987). However, two loci and alleles from one locus that display polymorphism have been discovered in bony fish. Thus, this discovery has disrupted the existing paradigm. In this article, different peptide-binding profiles originating from the products of the two different loci binding to the same MHC-I were illustrated, and the mechanism was elucidated by crystal structures of pMHC-I complexes.

As a result, a new paradigm has been established, which is well supported and has potential clinical value, for as various vertebrates have evolved, sharks (Venkatesh et al., 2014), amphibians (Session et al., 2016), reptiles (Organ et al., 2008), birds (Rubin et al., 2010) and mammals (Lappalainen et al., 2019) have retained only a single β2m locus, and the second β2m locus has been discovered only in bony fish. To verify that the second β2m locus is widespread among bony fish, we searched known genomic accessions of other bony fishes using known β2m sequences as queries and found that the majority of ray-finned fishes (e.g., common carp, large yellow croaker, channel catfish, and Japanese medaka) have the second β2m locus. It is generally thought that bony fishes underwent an additional WGD event, the bony fish-specific genome duplication (Cannon et al., 2002; Howe et al., 2013). Notably, a single copy of the β2m locus was found in the spotted gar; however, the gar diverged from bony fish before the occurrence of the TGD, suggesting

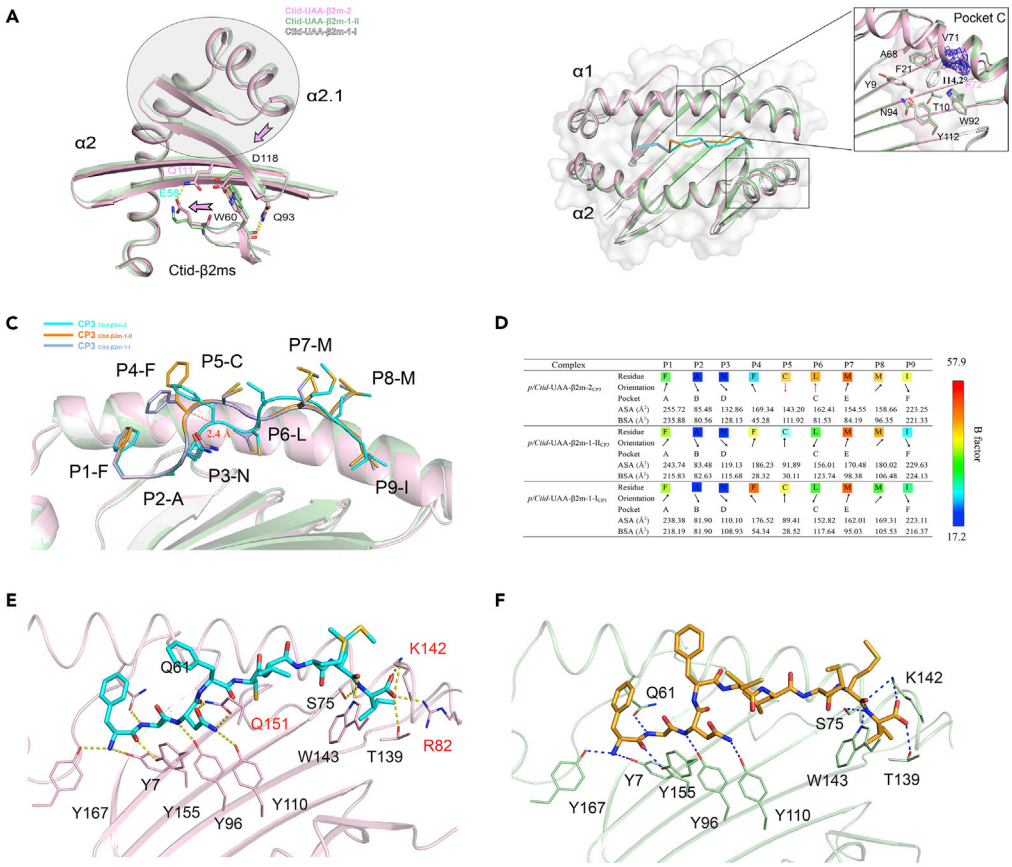

Complex		P1	P2	P3	P4	P5	P6	P7	P8	P9
p/Ctid-UAA-β2m-2$_{CP3}$	Residue	F	N	L	F	C	L	M	M	I
	Orientation	↗	↘	↘	↘	↑	↑	↗	↗	↘
	Pocket	A	B	D			C	E		F
	ASA (Å^2)	255.72	85.48	132.86	169.34	143.20	162.41	154.55	158.66	223.25
	BSA (Å^2)	235.88	80.56	128.13	45.28	111.92	81.53	84.19	96.35	221.33
p/Ctid-UAA-β2m-1-II$_{CP3}$	Residue	F	N	L	F	C	L	M	M	I
	Orientation	↗	↘	↘	↗	↑	↗	↗	↗	↘
	Pocket	A	B	D			C	E		F
	ASA (Å^2)	243.74	83.48	119.13	186.23	91.89	156.01	170.48	180.02	229.63
	BSA (Å^2)	215.83	82.63	115.68	28.32	30.11	123.74	98.38	106.48	224.13
p/Ctid-UAA-β2m-1-I$_{CP3}$	Residue	F	N	L	F	C	L	M	M	I
	Orientation	↗	↘	↘	↘	↑	↗	↗	↗	↘
	Pocket	A	B	D			C	E		F
	ASA (Å^2)	238.38	81.90	110.10	176.52	89.41	152.82	162.01	169.31	223.11
	BSA (Å^2)	218.19	81.90	108.93	54.34	28.52	117.64	95.03	105.53	216.37

Figure 5. Structural Changes in the PBG and the Different Conformations Caused by the Two Types of Ctid-β2ms

(A) Structural changes in the PBG of pCtid-UAA-β2m-2. In the two types of pCtid-UAA-β2m complexes, the regions involved in the structural changes in the PBG are superimposed. A unique hydrogen bond formed between the variable amino acids E58 and Q111 skews the DE loop, and the relative position of W60 correspondingly changes. However, the shaded area, namely, the α2.1 helix and the surrounding region, also shifts to the outside to maintain the overall stability of the PBG.

(B) A vertical view of the overlapping PBGs of the two types of pCtid-UAA-β2ms is shown in the cartoon and surface diagrams. In the pCtid-UAA-β2m complexes, a shift (~1.2 Å) of the α2.1 helix leads to relative position changes in T139, K142, and W143, which constitute the F pocket, and the C pocket deepens. In the boxed diagram, the residues involved in forming the C pocket are shown as sticks in the binding grooves of Ctid-UAA-β2m-2 (pink) and Ctid-UAA-β2m-1-I/II (white/light green).

(C) The peptide CP3 conformation in the two types of pCtid-UAA-β2ms. The Ctid-UAA-β2ms are shown in a cartoon model; Ctid-UAA-β2m-2 is shown in pink, Ctid-UAA-β2m-1-II is shown in light green, and Ctid-UAA-β2m-1-I is shown in white. The peptide CP3 is shown in the ribbon model; the peptide CP3 in Ctid-βm-2 is shown in cyan, the peptide CP3 in Ctid-βm-1-II is shown in orange, and the peptide CP3 in Ctid-βm-1-I is shown in light blue.

(D) General side chain orientations and the different interface areas of the peptide CP3 presented by the PBG of the two types of Ctid-UAA-β2ms, as viewed in profile from the peptide N terminus to the C terminus. The black arrows indicate the directions in which the residues point: up is toward the T cell receptor, down is toward the floor of the PBG, right is toward the α1 helix domain, and left is toward the α2 helix domain. The pockets accommodating each residue are listed under the corresponding anchors within the PBGs, and the numerical values of the accessible surface area (ASA) of each residue and buried surface area (BSA) of the residues are shown.

(E and F) Comparison of the interactions between the peptide CP3 and the residues of the PBG in the two types of Ctid-UAA-β2ms. The hydrogen bonds and salt bridges are shown as yellow dashed lines. The specific residue positions for interactions between the peptide CP3 and the PBG that differ from those of Ctid-UAA-β2m-1-I are labeled red in Ctid-UAA-β2m-2 and Ctid-UAA-β2m-1-II.

that the second type of β2m in bony fish might be derived from the TGD (Hoegg et al., 2004). Although the two *Ctid*-β2m loci have been found in the grass carp, it is hard to say which may be an ortholog of tetrapod β2ms. Given the teleost own genome duplications, the two Ctid-β2m genes probably diverged during the

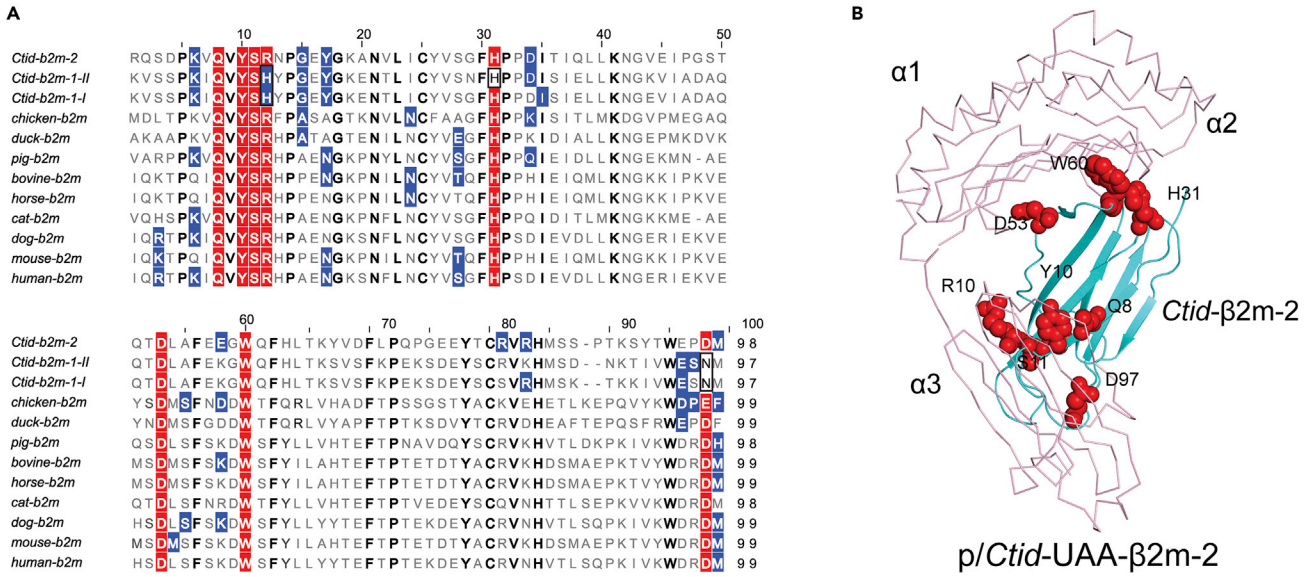

Figure 6. The Conserved Amino Acid Motifs of β2m Involved in Interaction with MHC-I Molecules in Known Different Vertebrates

(A) Multiple alignments of β2m amino acid sequences derived from known MHC class I complex structures (chicken PDB codes: 4GF2 and 3BEV; duck PDB code: 5GJX; pig PDB code: 5H94; bovine PDB code: 3QWU; horse PDB code: 4ZUS; cat PDB code: 5XMF; dog PDB code: 5F1I; mouse PDB codes: 1ZT1 and 1ZT7; human PDB code: IHHI). The amino acid sites involved in interactions with the MHC class I HC are shown in blue, whereas the eight conserved amino acid motifs (Q8, Y10, S11, R12, H31, D53, W60, and D97/98) are shown in red. The nonconserved amino acid sites of Ctid-β2m-1-I/II are shown in boxes. (B) The eight conserved amino acid sites (Q8, Y10, S11, R12, H31, D53, W60, and D97/98) on pCtid-UAA-β2m are shown as red spheres.

cyprinid genome duplication, well after the bony fish and tetrapod split, so they may be both equal orthologs.

The β2m is an essential component of the MHC class I antigen presentation pathway, and its main function is to participate in the pMHC-I interaction and maintain structural stability. Thus, a reasonable guess is that the amino acid sequences of β2ms involved in interactions with MHC-I molecule would have been conserved throughout the coevolutionary path and that these amino acids should be present in the two types of Ctid-β2ms. Based on the solved pMHC-I structures from the grass carp and other species, the eight conserved amino acid motifs (Q8, Y10, S11, R12, H31, D53, W60, and D97/98) of β2m involved in the interaction with the MHC-I molecules were found in mammalian and bird β2ms (Achour et al., 1998; Koch et al., 2007), although there was an exception, as D98 was substituted by an E, with the same charge, in the chicken. By contrast, Ctid-β2m-2 retained this conserved motif, compared with Ctid-β2m-1-I/II. Moreover, an interesting point also was found that in human CD8αα/MHC-I complexes, the contribution of β2m to CD8αα binding is relatively small and is mediated mainly by the K58 residue, which forms a vital salt bridge with D75 in CD8αα (Glick et al., 2002). A mutation from K58 to E58 can significantly reduce CD8αα binding and is a potent antagonist of CTL activation. In our study, two types of pCtid-UAA-β2m complexes and grass carp CD8αα homodimers were superimposed based on known HLA-A2-CD8αα complex structures (Figure S5) (Wang et al., 2018). From the perspective of sequence characterization, Ctid-β2m-2 is seemingly more suited than Ctid-β2m-1 to form a salt bridge with the grass carp CD8αα in the same position. Given the above, Ctid-β2m-2 seems to have more conserved features than Ctid-β2m-1. Although previous report showed that Ctid-β2m-1 has been shown to have a classical peptide presentation function through association with U-lineage MHC I in grass carp (Chen et al., 2010a, 2010b), it may also be worth noting that, in addition to U-lineage MHC I, other MHC I lineages and nonclassical MHC I molecules are also potential partners of the two types of Ctid-β2ms. From this point of view, a more intricate antigen-presenting mechanism mediated by the dual diversity and polymorphism of MHC I molecules and β2ms may exist in grass carp and even in other bony fishes than in mammals; however, further *in vivo* biological experiments may be needed to prove these assumptions.

In known pMHC-I structures, such as those from chickens and mammals, β2ms depend mainly on the D shift stabilizing the antigen-binding grooves, and a single β2m cannot change the structure the PBG, which does not affect the conformation of bound peptide. However, analysis of the structure of the pMHC-I formed by the two types of Ctid-β2m-1/-2 produced results that are quite different from those found for mammals. Ctid-

β2ms can combine with the same MHC-I in two forms, further affecting the conformation of PBGs and changing the peptide-binding profiles. Meanwhile, it can be rationally recognized that different antigen peptide profiles activate different T cell populations. The specific reason is that the amino acids on Ctid-β2m can bind to the amino acids at the bottom of the PBG, which results in a change in the F pocket and directly affects the conformation of the pocket-related region. We have found that β2ms with high homology can bind to an MHC-I across species (Yao et al., 2016) and that the peptide in pMHC-I formed by the same β2m has slight changes in the PBG (Li et al., 2011). However, this study is the first time that different β2ms binding to MHC-I in bony fish species have been shown to lead to changes in the conformation of the PBG. Here, the mechanism of the alteration of the peptide-binding profiles is also clearly explained. In addition to being an important event in MHC evolution and immunity, the clinical application value of these phenomena cannot be underestimated; changing the amino acid sequence of β2m can change the peptide-binding profile, which is of great significance in antivirus and antitumor function and avoidance of immune escape in humans.

Limitation of the Study

In this study, based on the *in vitro* phenomenon of variant peptide profiles with the participation of two types of β2m, we have expounded the structural mechanism of β2m changing the MHC-bound peptide presentation profile. Although our results have strongly supported the above mechanism in a diploid bony fish, whether it generally applies to all bony fishes still needs to be further explored through the genomic structures and sequences analysis. Another limitation of this study was the lack of the further *in vivo* biological experiments; we were unable to assess the situation in the body. Therefore, our results should be understood as a first glimpse into the complexity of teleost MHC-mediated cellular immunity and provided a possible way to change MHC-bound peptide presentation profile via β2m molecule in bony fish.

Resource Availability

Lead Contact

All relevant data and requests for resources and reagents should be directed to and will be fulfilled by the Lead Contact, Chun Xia (xiachun@cau.edu.cn).

Materials Availability

This study did not generate new unique reagents.

Data and Code Availability

Coordinates and structure factors have been deposited in the Protein Data Bank with accession codes 6LBE (Ctid-UAA-β2m-2) and 5H5Z (Ctid-UAA-β2m-1-II).

METHODS

All methods can be found in the accompanying Transparent Methods supplemental file.

DATA AND CODE AVAILABILITY

All relevant data and requests for resources and reagents should be directed to and will be fulfilled by the Lead Contact, Chun Xia (xiachun@cau.edu.cn). Coordinates and structure factors have been deposited in the Protein Data Bank with accession codes 6LBE (Ctid-UAA-β2m-2) and 5H5Z (Ctid-UAA-β2m-1-II).

SUPPLEMENTAL INFORMATION

Supplemental Information can be found online at https://doi.org/10.1016/j.isci.2020.101119.

ACKNOWLEDGMENTS

This work was supported by the National Natural Science Foundation of China (grant 31572653, grant 31572493). We acknowledge the assistance of the staff of the Shanghai Synchrotron Radiation Facility (SSRF) of China.

AUTHOR CONTRIBUTIONS

C.X. designed the study and supervised the project; Z.L. and L.M. performed all experiments and the data analysis; Z.L., L.Z., and G.M. solved the protein crystal structure; C.X. and N.Z. provided guidance on data analysis; Z.L. and L.M. wrote the paper; and C.X. revised the manuscript.

DECLARATION OF INTERESTS

The authors declare no competing interests.

Received: January 18, 2020
Revised: March 14, 2020
Accepted: April 28, 2020
Published: May 22, 2020

REFERENCES

Achour, A., Persson, K., Harris, R.A., Sundback, J., Sentman, C.L., Lindqvist, Y., Schneider, G., and Karre, K. (1998). The crystal structure of H-2Dd MHC class I complexed with the HIV-1-derived peptide P18-I10 at 2.4 A resolution: implications for T cell and NK cell recognition. Immunity *9*, 199–208.

Bjorkman, P.J., Saper, M.A., Samraoui, B., Bennett, W.S., Strominger, J.L., and Wiley, D.C. (1987). The foreign antigen binding site and T cell recognition regions of class I histocompatibility antigens. Nature *329*, 512–518.

Cannon, J.P., Haire, R.N., and Litman, G.W. (2002). Identification of diversified genes that contain immunoglobulin-like variable regions in a protochordate. Nature immunology *3*, 1200–1207.

Chen, W., Gao, F., Chu, F., Zhang, J., Gao, G.F., and Xia, C. (2010a). Crystal structure of a bony fish beta2-microglobulin: insights into the evolutionary origin of immunoglobulin superfamily constant molecules. J. Biol. Chem. *285*, 22505–22512.

Chen, W., Jia, Z., Zhang, T., Zhang, N., Lin, C., Gao, F., Wang, L., Li, X., Jiang, Y., Li, X., et al. (2010b). MHC class I presentation and regulation by IFN in bony fish determined by molecular analysis of the class I locus in grass carp. J. Immunol. *185*, 2209–2221.

Chen, Z., Zhang, N., Qi, J., Chen, R., Dijkstra, J.M., Li, X., Wang, Z., Wang, J., Wu, Y., and Xia, C. (2017). The structure of the MHC class I molecule of bony fishes provides insights into the conserved nature of the antigen-presenting system. J. Immunol. *199*, 3668–3678.

Cooper, M.D., and Alder, M.N. (2006). The evolution of adaptive immune systems. Cell *124*, 815–822.

Christie, D., Wei, G., Fujiki, K., and Dixon, B. (2007). Cloning and characterization of a cDNA encoding walleye (Sander vitreum) beta-2 microglobulin. Fish Shellfish Immunol. *22*, 727–733.

Dixon, B., Stet, R.J., van Erp, S.H., and Pohajdak, B. (1993). Characterization of beta 2-microglobulin transcripts from two teleost species. Immunogenetics *38*, 27–34.

Flajnik, M.F. (2018). A cold-blooded view of adaptive immunity. Nat. Rev. Immunol. *18*, 438–453.

Flajnik, M.F., and Kasahara, M. (2001). Comparative genomics of the MHC: glimpses into the evolution of the adaptive immune system. Immunity *15*, 351–362.

Gates, F.T., 3rd, Coligan, J.E., and Kindt, T.J. (1981). Complete amino acid sequence of murine beta 2-microglobulin: structural evidence for strain-related polymorphism. Proc. Natl. Acad. Sci. U S A *78*, 554–558.

Glick, M., Price, D.A., Vuidepot, A.L., Andersen, T.B., Hutchinson, S.L., Laugel, B., Sewell, A.K., Boulter, J.M., Dunbar, P.R., Cerundolo, V., et al. (2002). Novel CD8+ T cell antagonists based on beta 2-microglobulin. The Journal of biological chemistry *277*, 20840–20846.

Goodfellow, P.N., Jones, E.A., Van Heyningen, V., Solomon, E., Bobrow, M., Miggiano, V., and Bodmer, W.F. (1975). The beta2-microglobulin gene is on chromosome 15 and not in the HL-A region. Nature *254*, 267–269.

Grimholt, U. (2018). Whole genome duplications have provided teleosts with many roads to peptide loaded MHC class I molecules. BMC Evol. Biol. *18*, 25.

Grimholt, U. (2016). MHC and evolution in teleosts. Biology *5*, 6.

Hao, H.F., Yang, T.Y., Yan, R.Q., Gao, F.S., and Xia, C. (2006). cDNA cloning and genomic structure of grass carp (Ctenophayngodon idellus) beta2-microglobulin gene. Fish Shellfish Immunol. *20*, 118–123.

Hoegg, S., Brinkmann, H., Taylor, J.S., and Meyer, A. (2004). Phylogenetic timing of the fish-specific genome duplication correlates with the diversification of teleost fish. Journal of molecular evolution *59*, 190–203.

Howe, K., Clark, M.D., Torroja, C.F., Torrance, J., Berthelot, C., Muffato, M., Collins, J.E., Humphray, S., McLaren, K., Matthews, L., et al. (2013). The zebrafish reference genome sequence and its relationship to the human genome. Nature *496*, 498–503.

Hurlbut, J.B. (2019). Human genome editing: ask whether, not how. Nature *565*, 135.

International Chicken Genome Sequencing Consortium. (2004). Sequence and comparative analysis of the chicken genome provide unique perspectives on vertebrate evolution. Nature *432*, 695–716.

Jondal, M., Schirmbeck, R., and Reimann, J. (1996). MHC class I-restricted CTL responses to exogenous antigens. Immunity *5*, 295–302.

Koch, M., Camp, S., Collen, T., Avila, D., Salomonsen, J., Wallny, H.J., van Hateren, A., Hunt, L., Jacob, J.P., Johnston, F., et al. (2007). Structures of an MHC class I molecule from B21 chickens illustrate promiscuous peptide binding. Immunity *27*, 885–899.

Kondo, H., Darawiroj, D., Gung, Y.T., Yasuike, M., Hirono, I., and Aoki, T. (2010). Identification of two distinct types of beta-2 microglobulin in marine fish, *Pagrus major* and *Seriola quinqueradiata*. Vet. Immunol. Immunopathol. *134*, 284–288.

Kumar, S., and Hedges, S.B. (1998). A molecular timescale for vertebrate evolution. Nature *392*, 917–920.

Lancet, D., Parham, P., and Strominger, J.L. (1979). Heavy chain of HLA-A and HLA-B antigens is conformationally labile: a possible role for beta 2-microglobulin. Proc. Natl. Acad. Sci. U S A *76*, 3844–3848.

Lappalainen, T., Scott, A.J., Brandt, M., and Hall, I.M. (2019). Genomic analysis in the age of human genome sequencing. Cell *177*, 70–84.

Li, X., Liu, J., Qi, J., Gao, F., Li, Q., Li, X., Zhang, N., Xia, C., and Gao, G.F. (2011). Two distinct conformations of a rinderpest virus epitope presented by bovine major histocompatibility complex class I N*01801: a host strategy to present featured peptides. J. Virol. *85*, 6038–6048.

Lundqvist, M.L., Appelkvist, P., Hermsen, T., Pilstrom, L., and Stet, R.J. (1999). Characterization of beta2-microglobulin in a primitive fish, the Siberian sturgeon (*Acipenser baeri*). Immunogenetics *50*, 79–83.

Magor, K.E., Shum, B.P., and Parham, P. (2004). The beta 2-microglobulin locus of rainbow trout (*Oncorhynchus mykiss*) contains three polymorphic genes. J. Immunol. *172*, 3635–3643.

Ohta, Y., Shiina, T., Lohr, R.L., Hosomichi, K., Pollin, T.I., Heist, E.J., Suzuki, S., Inoko, H., and Flajnik, M.F. (2011). Primordial linkage of beta2-microglobulin to the MHC. J. Immunol. *186*, 3563–3571.

Ono, H., Figueroa, F., O'HUigin, C., and Klein, J. (1993). Cloning of the beta 2-microglobulin gene in the zebrafish. Immunogenetics *38*, 1–10.

Organ, C.L., Moreno, R.G., and Edwards, S.V. (2008). Three tiers of genome evolution in reptiles. Integr. Comp. Biol. *48*, 494–504.

Robinson, P.J., Graf, L., and Sege, K. (1981). Two allelic forms of mouse beta 2-microglobulin. Proc. Natl. Acad. Sci. U S A *78*, 1167–1170.

Rubin, C.J., Zody, M.C., Eriksson, J., Meadows, J.R., Sherwood, E., Webster, M.T., Jiang, L., Ingman, M., Sharpe, T., Ka, S., et al. (2010). Whole-genome resequencing reveals loci under selection during chicken domestication. Nature *464*, 587–591.

Session, A.M., Uno, Y., Kwon, T., Chapman, J.A., Toyoda, A., Takahashi, S., Fukui, A., Hikosaka, A., Suzuki, A., Kondo, M., et al. (2016). Genome evolution in the allotetraploid frog Xenopus laevis. Nature *538*, 336–343.

Sever, L., Vo, N.T., Lumsden, J., Bols, N.C., and Dixon, B. (2014). Induction of rainbow trout MH class I and accessory proteins by viral haemorrhagic septicaemia virus. Mol. Immunol. *59*, 154–162.

Shum, B.P., Azumi, K., Zhang, S., Kehrer, S.R., Raison, R.L., Detrich, H.W., and Parham, P. (1996). Unexpected beta2-microglobulin sequence diversity in individual rainbow trout. Proc. Natl. Acad. Sci. U S A *93*, 2779–2784.

Simister, N.E., and Mostov, K.E. (1989). An Fc receptor structurally related to MHC class I antigens. Nature *337*, 184–187.

Venkatesh, B., Lee, A.P., Ravi, V., Maurya, A.K., Lian, M.M., Swann, J.B., Ohta, Y., Flajnik, M.F., Sutoh, Y., Kasahara, M., et al. (2014). Elephant shark genome provides unique insights into gnathostome evolution. Nature *505*, 174–179.

Wang, Y., Lu, Y., Zhang, Y., Ning, Z., Li, Y., Zhao, Q., Lu, H., Huang, R., Xia, X., Feng, Q., et al. (2015). The draft genome of the grass carp (*Ctenopharyngodon idellus*) provides insights into its evolution and vegetarian adaptation. Nat. Genet. *47*, 625–631.

Wang, J., Zhang, N., Wang, Z., Yanan, W., Zhang, L., and Xia, C. (2018). Structural insights into the evolution feature of a bony fish CD8alphaalpha homodimer. Molecular immunology *97*, 109–116.

Xu, P., Zhang, X., Wang, X., Li, J., Liu, G., Kuang, Y., Xu, J., Zheng, X., Ren, L., Wang, G., et al. (2014). Genome sequence and genetic diversity of the common carp, *Cyprinus carpio*. Nat. Genet. *46*, 1212–1219.

Yao, S., Liu, J., Qi, J., Chen, R., Zhang, N., Liu, Y., Wang, J., Wu, Y., Gao, G.F., and Xia, C. (2016). Structural illumination of equine MHC class I molecules highlights unconventional epitope presentation manner that is evolved in equine leukocyte antigen alleles. J. Immunol. *196*, 1943–1954.

Zhang, C.M., Yamaguchi, K., So, M., Sasahara, K., Ito, T., Yamamoto, S., Narita, I., Kardos, J., Naiki, H., and Goto, Y. (2019). Possible mechanisms of polyphosphate-induced amyloid fibril formation of beta2-microglobulin. Proc. Natl. Acad. Sci. U S A *116*, 12833–12838.

iScience, Volume *23*

Supplemental Information

The Mechanism of β2m Molecule-Induced Changes in the Peptide Presentation Profile in a Bony Fish

Zibin Li, Nianzhi Zhang, Lizhen Ma, Lijie Zhang, Geng Meng, and Chun Xia

SUPPLEMENTAL ITEMS

FIGURE

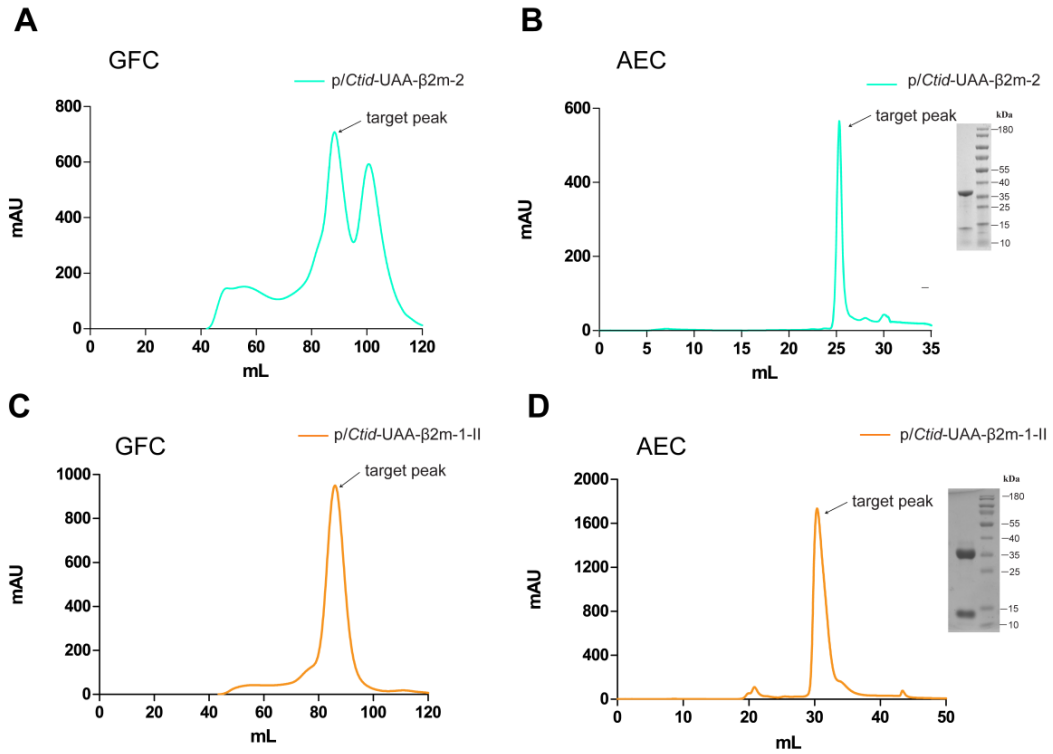

Figure S1. Refolding efficiency of pCtid-UAA-β2m-2 and pCtid-UAA-β2m-1-II, Related to Figure 3. Ctid-β2m-2 and Ctid-β2m-1-II were expressed and corefolded with Ctid-UAA and the peptide CP3. The pCtid-UAA-β2m-2 and pCtid-UAA-β2m-1-II curves are shown in cyan and orange, respectively. The target peak of the pMHC-I complex is indicated by an arrow. The insets show reducing SDS-PAGE gels (15%) of the target peaks labeled on the curve. Lane M contains molecular mass markers (labeled in kDa). (A and C) Gel filtration chromatograms of the refolded products. (B and D) Anion exchange chromatograms of the refolded products.

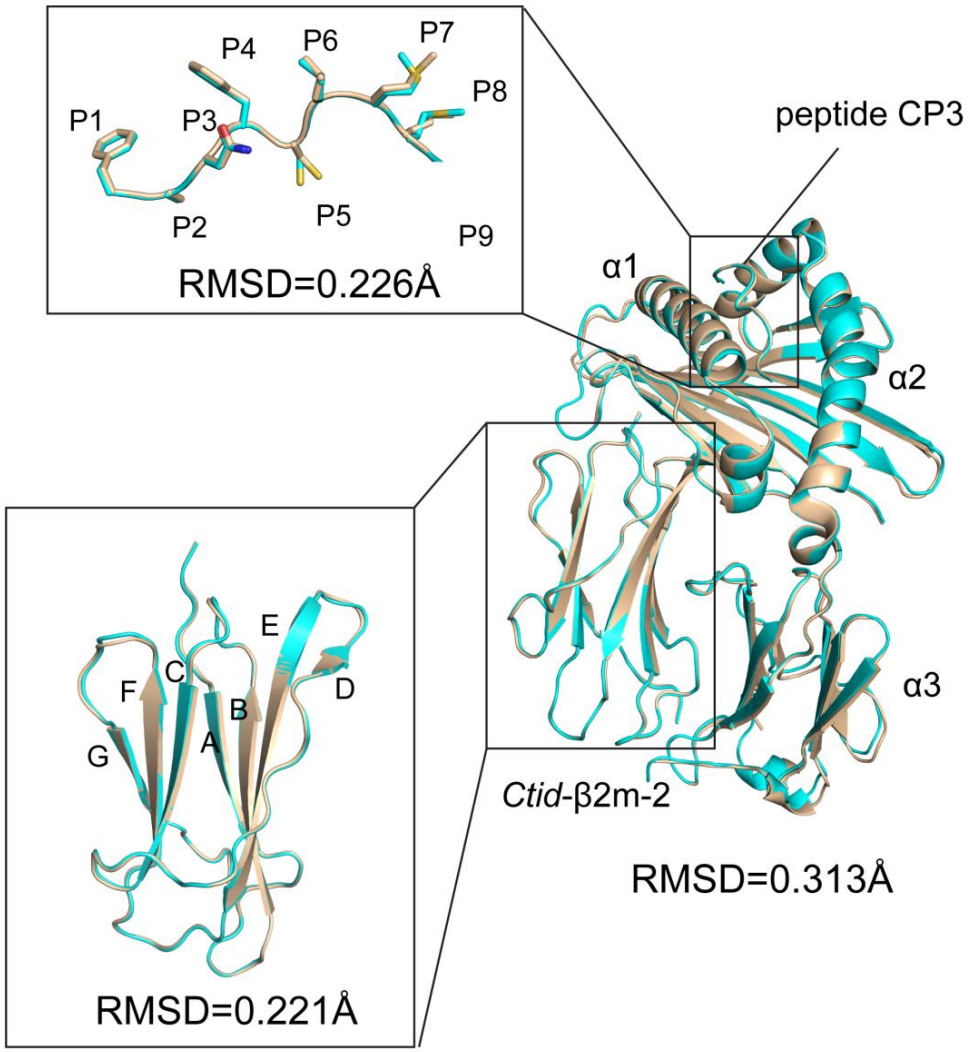

Figure S2. Two pCtid-UAA-β2m-2 complexes in the asymmetric unit are superimposed, and the two complexes are essentially identical, Related to Figure 3. The corresponding domains of the two complexes are highlighted. All atoms of the two complexes were superimposed with an RMSD of 0.298, the peptide CP3 backbones were superimposed with an RMSD of 0.250, and the Ctid-β2m-2 backbones were superimposed with an RMSD of 0.178.

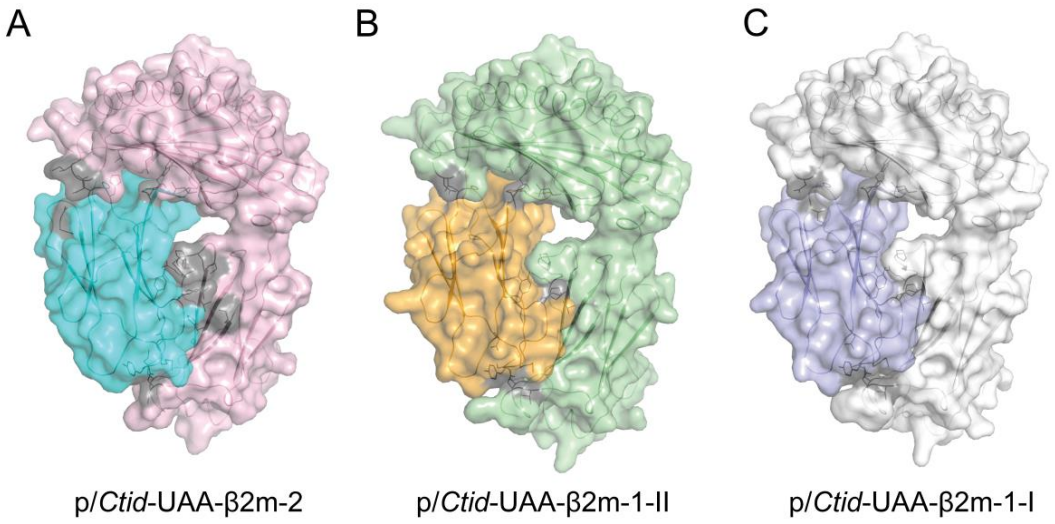

Figure S3. Comparison of the interface areas of the heavy chain and light chains in the two types of pCtid-UAA-β2ms, Related to Figure 4.

(A) Interface areas of the HC and LCs in pCtid-UAA-β2m-2. The Ctid-UAA HC and the Ctid-β2m-2 LC are shown as surface cartoons and are colored pink and cyan, respectively.

(B) Interface areas of the HC and LCs in the pCtid-UAA-β2m-1-II complex. The Ctid-UAA HC and the Ctid-β2m-1-II LC are shown as surface cartoons and are colored light green and orange, respectively.

(C) Interface areas of the HC and LCs in the pCtid-UAA-β2m-1-I complex. The Ctid-UAA HC and the Ctid-β2m-1-I LC are shown as surface cartoons and are colored white and light blue, respectively. All interacting residues of the HCs and LCs are shown as gray sticks.

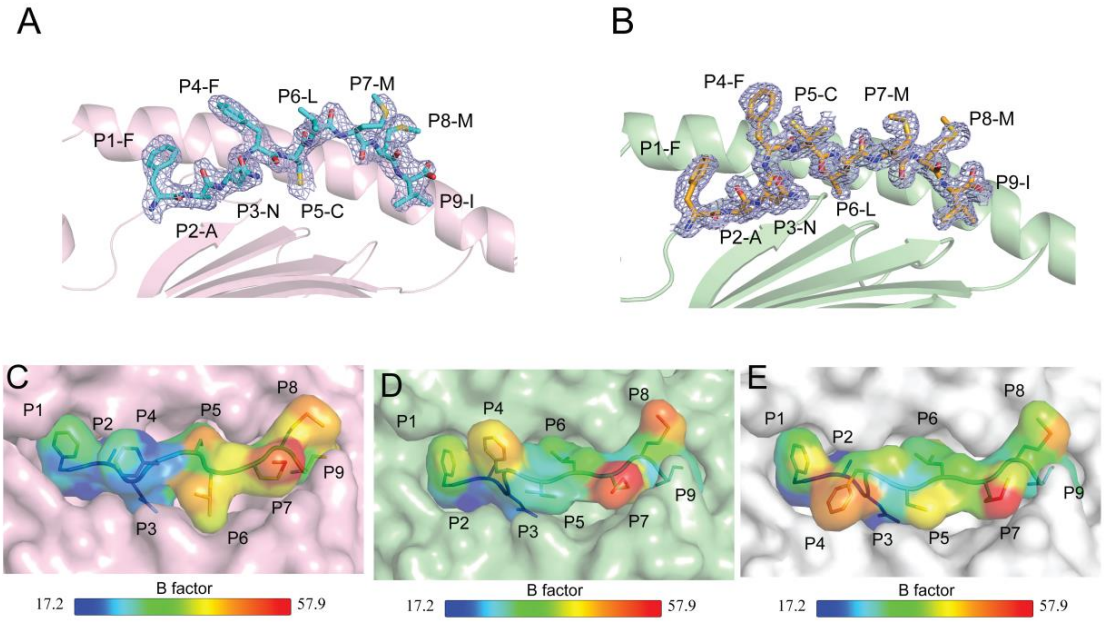

Figure S4. Details of peptide CP3 in the two types of pCtid-UAA-β2ms, Related to Figure 5.

(A and B) The peptide CP3 β2m-2 (cyan) and the peptide CP3β2m-1-I (orange) in the structures of Ctid-UAA-β2m-2 (pink) and Ctid-UAA-β2m-1-II (light green) are presented with the 2F0–Fc electron density maps at the 1.0 σ contour level. The residues in the peptides are denoted with individual letters and position numbers.

(C and D) Comparison of the interactions between the peptide CP3 and the residues of the PBG in the two types of Ctid-UAA-β2ms. The hydrogen bonds and salt bridges are shown as yellow dashed lines. The specific residue positions for interactions between the peptide CP3 and the PBG that differ from those of Ctid-UAA-β2m-1-I are labeled red in Ctid-UAA-β2m-2 and Ctid-UAA-β2m-1-II.

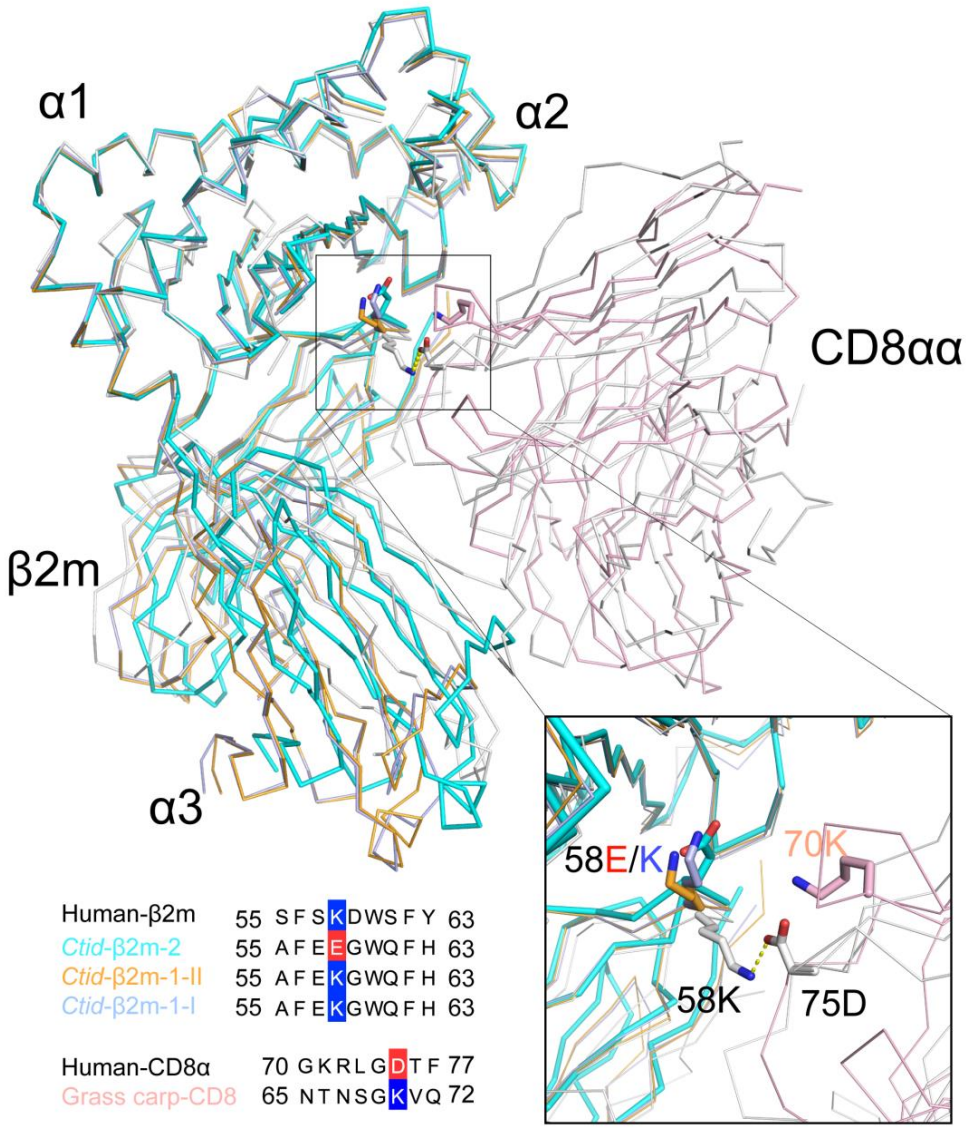

Figure S5. The two types of pCtid-UAA-β2ms binding to grass carp CD8αα homodimer, Related to Figure 6. pCtid-UAA-β2m-2 (cyan), pCtid-UAA-β2m-1-II (orange), pCtid-UAA-β2m-1-I (light blue) and the grass carp CD8αα homodimer structure (pink, PDB code: 5Z11) are superimposed onto the HLA-A2-CD8αα structure (white, PDB code: 1AKJ). All structures are shown in ribbon form and labeled with corresponding colors. Residue K58 (stick, white) on the human β2m forms a key salt bridge with residue D75 (stick, white) on the human CD8αα molecule. In the three pCtid-UAA-β2m complexes, as the residues E/K58 (stick, red/blue) and K70 (stick, pink) reside on Ctid-β2m-2/Ctid-β2m-1-I/II and the grass carp CD8αα, respectively, the same salt bridge is most likely to form between the pCtid-UAA-β2m-2 complex and the grass carp CD8αα molecule.

TABLE

Table S1. Alleles expressed in the cDNA of each grass carp individual, Related to Figure 1.

Individual	Names	Alleles	Accession numbers	Subgroup	Corresponding Structure sequence
1	***Ctid*-β2m-0101**	**a05**	**MG902917**	I	
	***Ctid*-β2m-0102**	**a02**	**MG902920**	II	*Ctid*-β2m-1-II
2	*Ctid*-β2m-0201	a05	MG902917	I	
	Ctid-β2m-0202	a02	MG902920	II	
3	***Ctid*-β2m-0301**	**a06**	**MG902921**	II	
	Ctid-β2m-0302	a02	MG902920	II	
4	***Ctid*-β2m-0401**	**a01**	**AB198014**	I	
	Ctid-β2m-0402	**a03**	**MG902924**	I	
5	Ctid-β2m-0501	a03	MG902924	I	
	Ctid-β2m-0502	a01	AB198014	I	*Ctid*-β2m-1-I
6	***Ctid*-β2m-0601**	**a07**	**MG902927**	II	
	***Ctid*-β2m-0602**	**a08**	**MG902928**	II	
7	Ctid-β2m-0701	a08	MG902928	II	
	Ctid-β2m-0702	a06	MG902921	II	
8	***Ctid*-β2m-0801**	**a09**	**MG902931**	II	
	***Ctid*-β2m-0802**	**a04**	**MG902932**	I	
9	*Ctid*-β2m-0901	a08	MG902928	II	
	Ctid-β2m-0902	a04	MG902932	I	
10	*Ctid*-β2m-1001	a09	MG902931	II	
	Ctid-β2m-1002	a03	MG902924	I	
11	*Ctid*-β2m-1101	a03	MG902924	I	
	Ctid-β2m-1102	a09	MG902931	II	
1-11	*Ctid*-β2m-2	—	MH882722	—	*Ctid*-β2m-2

Shared alleles are indicated in bold.

Table S3. Hydrogen bonds interactions between *Ctid*-β2ms and *Ctid*-UAA, Related to Figure 4.

Types of *Ctid*-β2m	Number	*Ctid*-β2m	Atoms	Dist.[Å]	*Ctid*-UAA	Atoms
	1	K6	[NZ]	2.82	E225	[OE1]
	2	Y10	[OH]	2.64	P228	[O]
	3	S11	[O]	3.07	Q235	[NE2]
	4	**R12**	**[NH1]**	**3.42**	**Q182**	**[OE1]**
	5	**R12**	**[O]**	**2.76**	**T199**	**[OG1]**
	6	**R12**	**[NH2]**	**2.66**	**D231**	**[OD2]**
	7	**R12**	**[NH2]**	**3.55**	**S233**	**[OG]**
	8	**R12**	**[O]**	**3.20**	**Q235**	**[NE2]**
***Ctid*-β2m-2**	9	G15	[O]	2.71	Q273	[ND2]
	10	Y17	[N]	3.14	Q273	[OD1]
	11	**H31**	**[NE2]**	**3.05**	**T91**	**[OG1]**
	12	**D34**	**[OD2]**	**2.65**	**I16**	**[N]**
	13	**D34**	**[OD1]**	**3.03**	**D17**	**[N]**
	14	**D34**	**[OD1]**	**3.71**	**F18**	**[N]**
	15	I35	[N]	3.67	D17	[OD2]
	16	**D53**	**[OD2]**	**2.68**	**Q31**	**[NE2]**
	17	**D53**	**[OD2]**	**3.52**	**K45**	**[NZ]**
	18	E58	[OE2]	3.23	Q111	[NE2]
	19	W60	[O]	3.51	Q93	[NE2]
	20	W60	[NE1]	2.53	D118	[OD1]
	21	**R83**	**[NH1]**	**3.71**	**D17**	**[OD2]**
	22	R83	[NH2]	3.12	D17	[OD1]
	23	D97	[OD1]	3.49	K188	[NZ]
	24	**M98**	**[O]**	**3.00**	**N273**	**[ND2]**
	1	K6	[NZ]	3.2	E225	[OE1]
	2	K6	[NZ]	3.38	E225	[OE2]
	3	Q8	[NH2]	3.4	E225	[O]
	4	Y10	[OH]	2.59	P228	[O]
	5	S11	[O]	2.87	Q235	[NE2]
	6	H12	[O]	2.87	Q235	[NE2]
	7	H12	[O]	2.72	T199	[OG1]
	8	G15	[O]	2.91	N273	[ND2]
	9	Y17	[N]	3.1	N273	[OD1]
	10	**D34**	**[OD2]**	**3.72**	**D17**	**[N]**
	11	D53	[O]	3.3	Q31	[OD1]
***Ctid*-β2m-1-II**	12	W60	[NH1]	2.73	D118	[OD1]

	13	W60	[O]	2.89	Q93	[NE2]
	14	E94	[OE2]	2.71	K188	[NZ]
	15	**S95**	**[OG]**	**3.31**	**K188**	**[NZ]**
	16	**M97**	**[OXT]**	**2.88**	**K189**	**[NZ]**
	17	M97	[O]	3.2	T272	[OG1]
	18	M97	[O]	2.85	N273	[N]
	1	K6	[NZ]	2.93	E225	[OE1]
	2	K6	[NZ]	3.22	E225	[OE2]
	3	Q8	[NE2]	3.42	E225	[OE2]
	4	Y10	[OH]	2.66	P228	[O]
	5	S11	[O]	2.97	Q235	[NE2]
	6	H12	[O]	3.53	Q235	[NE2]
	7	H12	[O]	2.8	T199	[OG1]
	8	G15	[O]	2.96	N273	[ND2]
	9	Y17	[N]	3.2	N273	[OD1]
	10	I35	[N]	2.96	D17	[OD1]
***Ctid*-β2m-1-I**	11	D53	[O]	3.4	Q31	[OD1]
	12	W60	[NE1]	2.64	D118	[OD1]
	13	W60	[O]	2.84	Q93	[NE2]
	14	R83	[NH2]	3.48	D17	[OD1]
	15	E94	[OE2]	2.89	K188	[NZ]
	16	M97	[O]	2.98	T272	[OG1]

Different hydrogen bonds interactions with *Ctid*-β2ms are indicated in bold.

Table S4. Salt bridges between the *Ctid*-β2m and *Ctid*-UAA, Related to Figure 4.

Types of *Ctid*-β2m	Number	*Ctid*-β2m	Atoms	Dist.[Å]	*Ctid*-UAA	Atoms
	1	K6	[NZ]	3.71	Q225	[OE1]
	2	K6	[NZ]	3.12	Q225	[OE2]
	3	R12	[NE]	3.32	Q230	[OE1]
	4	R12	[NE]	3.52	Q230	[OE2]
***Ctid*-β2m-2**	**5**	R12	[NE]	3.49	D231	[OD2]
	6	R12	[NH2]	2.82	D231	[OD1]
	7	R12	[NH2]	3.78	D231	[OD2]
	8	D53	[OD2]	3.26	K45	[NZ]
	9	R83	[NH1]	3.46	D17	[OD2]
	10	R83	[NH2]	3.31	D17	[OD1]
	11	R83	[NH2]	3.76	D17	[OD2]
	12	D97	[OD1]	2.66	K188	[NZ]
	1	K6	[NZ]	3.2	E225	[OE1]
***Ctid*-β2m-1-II**	2	K6	[NZ]	3.38	E225	[OE2]
	3	E94	[OE2]	2.71	K188	[NZ]
	1	K6	[NZ]	2.93	E225	[OE1]
***Ctid*-β2m-1-I**	2	K6	[NZ]	3.22	E225	[OE2]
	3	R83	[NH2]	3.48	D17	[OD1]
	4	E94	[OE2]	2.89	K188	[NZ]

Different salt bridges interactions with *Ctid*-β2ms are indicated in bold.

Table S5. qPCR and polymorphic analysis primers specific for grass carp β2m genes, Related to Figure 1.

Name	Sequences	Product length (bp)	Ta(℃)
Ctid-b2m-15'qFOR	CTGGTGTTTCTAAGCGCC	94	60
Ctid-b2m-13'qREV	CGTTTGCTTTCCCATACTCTC		
Ctid-b2m-25'qFOR	TGCTGAAGAATGGAGAGGTTAT	99	60
Ctid-b2m-23'qREV	GTTTGAAGGAGACGCTCTTG		
18SRNA5'qFOR	ATTTCCGACACGGAGAGG	90	60
18SRNA3'qREV	CATGGGTTTAGGATACGCTC		
Ctid-β2m-15'FOR	ATGCGAGCACTCGTCTCTTTTGTGT		
Ctid-β2m-13'REV	GTTAGCTTTACATGTTGGACTCCCA		
Ctid-β2m-25'FOR	ATGTGGTTCAAACTCGCTGTAGTCGCGCT		
Ctid-β2m-23'REV	TCACATGTCAGGCTCCCACGTGTAGGACT		

Transparent Methods

Phylogenetic analysis of Ctid-β2ms

Eleven outbred grass carp individuals were obtained from the Yangtze River in China (Li et al., 2019). In brief, different tissues (kidney, skin, liver, spleen, heart, intestine and gill) were collected, and blood (100 μl to 1 ml) was taken from the caudal vein using a heparinized syringe with a 23 G needle. The blood cells were washed with PBS and resuspended in up to 1 ml of RPMI 1640 medium with 10% DMSO. The tissues and blood cells were stored at -80 °C for follow-up total RNA extraction. According to a standard protocol, total RNA from the blood was extracted using TRIzol reagent, and the RNA concentrations were measured by spectrophotometry. The RNA was then reverse transcribed into cDNA using an ExScript RT Reagent Kit. The two Ctid-β2m genes were cloned according to previously reported methods (Shum et al., 1996). The already-known Ctid-β2m gene was named Ctid-β2m-1, and the second Ctid-β2m gene was named Ctid-β2m-2. The primers used are listed in Table S5. The obtained Ctid-β2m allele sequences were submitted to GenBank (National Center for Biotechnology Information: https://www.ncbi.nlm.nih.gov/genbank/).

The Ctid-β2m-1 and Ctid-β2m-2 alleles were subjected to multiple sequence alignments via the ClustalW (ver. 1.83) and Jalview (ver. 1.2) programs. A phylogenetic tree was constructed with the MEGA 6 program using the neighbor-joining method with 1000 bootstrap replicates. The evolutionary distance in nucleotides was estimated with the Kimura 2-parameter method in MEGA 6(Kimura, 1980).

Tissue distribution of the two Ctid-β2m genes

Total RNA from the different tissues of the grass carp was reverse transcribed using M-MLV SuperScript reverse transcriptase according to the manufacturer's instructions. Real-time PCR was performed using QuantiFast® SYBR® Green PCR Master Mix (Qiagen, Germany) and a LightCycler® 480 II Real-time PCR Instrument (Roche, Switzerland). The primers used are listed in Table S5. The mRNA expression levels were normalized to 18S rRNA expression and were calculated using the 2-ΔΔCt method (Schmittgen and Livak, 2008).

Synthesis of peptides and a completely random nonapeptide library

The CP3 peptide (SVCV-FAN9, FANFCLMMI), which was used in our previous experiments(Chen et al., 2017), and a completely random nonapeptide library (X×9) in which there was an equal representation of the 20 amino acids at each position, were synthesized by SciLight Biotechnology (Beijing, China). The purity of all synthesized peptides was >90%, as assessed using reverse-phase HPLC (SciLight Biotechnology).

Assembly of pCtid-UAA-β2m-2 and pCtid-UAA-β2m-1-II

The mature peptide sequences of Ctid-β2m-2 (amino acids 1-99), Ctid-β2m-1-II (amino acids 1-98) and Ctid-UAA (amino acids 1-276) were inserted into the pET21a vector and expressed in BL21 (DE3) E. coli. The recombinant proteins were expressed as inclusion bodies and then purified according to previously described methods. The Ctid-UAA, Ctid-β2m-2/1-II and peptide CP3 complexes were refolded and purified following previously described methods(Chen et al., 2017).

Random nonapeptide library in vitro binding assays

The two types of pCtid-UAA-β2m complexes bound to random nonapeptides were refolded in vitro and

purified according to the above methods for the assembly of the pCtid-UAA-β2m complex. The peptide ligands were dissociated from the purified complexes with a weak acid treatment method(Storkus et al., 1993). After concentration, the peptide ligands were identified with an EASY nLC 1000 liquid chromatography-tandem mass spectrometry (LC-MS/MS) system (Thermo Fisher, San Jose). First, the desalted peptide ligands were separated with a C18 column at a flow rate of 400 nl/min. A linear gradient was set as follows: 1% B (0.1% formic acid (FA) in acetonitrile (ACN) (v/v)/99% A (0.1% FA in H2O (v/v))) to 5% B in 1 minute, 5% B to 30% B in 89 minutes, 30% B to 40% B in 2 minutes, 40% B to 90% B in 3 minutes, maintenance at 90% for 10 minutes, and column re-equilibration at 1% B for 14 minutes. Mass spectrometry (MS) data were acquired using a data-dependent acquisition mode with Q Exactive (Thermo Fisher, Bremen), and 20 precursors with the highest intensity in the mass range 300 to 1800 m/z were sequentially fragmented with higher-energy collision dissociation (HCD) with a normalized collision energy (NCE) of 27. The resolution for the MS1 and MS2 scans was set to 70k and 17.5k, respectively, and the automatic gain control (AGC) for MS1 and MS2 was set to 3e6 and 5e5, respectively. The dynamic exclusion time was 20 s. The obtained raw files were processed using PEAKS Studio software with precursor and fragment mass tolerances of 10 ppm and 0.02 Da, respectively. The variable modification was set to the oxidation of M and the deamidation of N and Q; de novo peptide ligands with amino acid sequence lengths of 9 and average local confidence (ALC) scores ≥50 were filtered. The nonapeptide ligands ultimately obtained from the two types of pCtid-UAA-β2ms were analyzed with Seq2Logo 2.1 (http://www.cbs.dtu.dk/biotools/Seq2Logo-2.1/)(Komnatnyy et al., 2012).

Crystallization, data collection, and structure determination

pCtid-UAA-β2m-2 and pCtid-UAA-β2m-1-II were crystallized by the sitting drop vapor diffusion method. pCtid-UAA-β2m-2 and pCtid-UAA-β2m-1-II (1 μl at 4 mg/ml and 10 mg/ml, respectively) in 20 mM Tris (pH 8.0) and 50 mM NaCl were mixed with 1 μl of reservoir solution (pCtid-UAA-β2m-2: 0.2 M ammonium sulfate, 0.1 M bis-Tris pH 6.5, 25% polyethylene glycol 3350; pCtid-UAA-β2m-1-II: 0.2 M sodium citrate tribasic dehydrate, 20% w/v polyethylene glycol 3350) at 4 °C and 18 °C, respectively. The pCtid-UAA-β2m-2 and pCtid-UAA-β2m-1-II crystals were cryoprotected in mother liquor by the addition of 20% glycerol before being flash cooled at 100 K. Diffraction data for pCtid-UAA-β2m-2 and pCtid-UAA-β2m-1-II were collected at the beamline BL17U at the Shanghai Synchrotron Radiation Facility (SSRF). The collected intensities were indexed, integrated, corrected for absorption, and then scaled and merged using HKL-2000(Otwinowski and Minor, 1997). The pCtid-UAA-β2m-2 and pCtid-UAA-β2m-1-II structures were solved by molecular replacement using Phaser from the CCP4 program suite(Collaborative Computational Project, 1994) with the structure of pCtid-UAA-β2m-1-I (Protein Data Bank (PDB) code: 5Y91) as the search model. The initial model was refined by rigid-body refinement using REFMAC5(Murshudov et al., 1997), and extensive model building was performed using COOT(Emsley and Cowtan, 2004). Further rounds of refinement were performed using the phenix.refine program implemented in the PHENIX package(Adams et al., 2010), with energy minimization, isotropic atomic displacement parameter (ADP) refinement, and bulk solvent modeling. The final statistics for the pCtid-UAA-β2m-2 and pCtid-UAA-β2m-1-II structures are represented in Table 1. The stereochemical quality of the final model was assessed with the program PROCHECK.

REFERENCES

Adams, P.D., Afonine, P.V., Bunkoczi, G., Chen, V.B., Davis, I.W., Echols, N., Headd, J.J., Hung, L.W., Kapral, G.J., Grosse-Kunstleve, R.W.*, et al.* (2010). PHENIX: a comprehensive Python-based system for macromolecular structure solution. Acta crystallographica. Section D, Biological crystallography *66*, 213-221.

Collaborative Computational Project, N. (1994). The CCP4 suite: programs for protein crystallography. Acta crystallographica. Section D, Biological crystallography *50,* 760-763.

Emsley, P., and Cowtan, K. (2004). Coot: model-building tools for molecular graphics. Acta crystallographica. Section D, Biological crystallography *60*, 2126-2132.

Li, Z., Zhang, N., Ma, L., Qu, Z., Wei, X., Liu, Z., Tang, M., Zhang, N., Jiang, Y., and Xia, C. (2019). Distribution of ancient alpha1 and alpha2 domain lineages between two classical MHC class I genes and their alleles in grass carp. Immunogenetics *71*, 395-405.

Murshudov, G.N., Vagin, A.A., and Dodson, E.J. (1997). Refinement of macromolecular structures by the maximum-likelihood method. Acta crystallographica. Section D, Biological crystallography *53*, 240-255.

Kimura, M. (1980). A simple method for estimating evolutionary rates of base substitutions through comparative studies of nucleotide sequences. Journal of molecular evolution *16*, 111-120.

Komnatnyy, V.V., Givskov, M., and Nielsen, T.E. (2012). Solid-phase synthesis of structurally diverse heterocycles by an amide-ketone condensation/N-acyliminium pictet-spengler sequence. Chemistry *18*, 16793-16800.

Otwinowski, Z., and Minor, W. (1997). Processing of X-ray diffraction data collected in oscillation mode. Methods in enzymology *276*, 307-326.

Schmittgen, T.D., and Livak, K.J. (2008). Analyzing real-time PCR data by the comparative C(T) method. Nature protocols *3*, 1101-1108.

Storkus, W.J., Zeh, H.J., 3rd, Salter, R.D., and Lotze, M.T. (1993). Identification of T-cell epitopes: rapid isolation of class I-presented peptides from viable cells by mild acid elution. Journal of immunotherapy with emphasis on tumor immunology : official journal of the Society for Biological Therapy *14*, 94-103.